# Petrology of Lower Crustal and Upper Mantle Xenoliths from the Cima Volcanic Field, California

*by* H. G. WILSHIRE[1], ANNE V. McGUIRE[2], J. S. NOLLER[3] AND B. D. TURRIN[1]

[1]*U.S. Geological Survey, Menlo Park, California 94025*
[2]*University of Houston, Houston, Texas 77004*
[3]*U.S. Geological Survey, Denver, Colorado 80225*

## ABSTRACT

Basaltic rocks of the Cima volcanic field in the southern Basin and Range province contain abundant gabbro, pyroxenite, and peridotite xenoliths. Composite xenoliths containing two or more rock types show that upper-mantle spinel peridotite was enriched by multiple dike intrusions in at least three episodes; the mantle was further enriched by intergranular and shear-zone melt infiltration in at least two episodes. The oldest dikes, now metamorphosed, are Cr-diopside websterite. Dikes of intermediate age are most abundant at Cima and consist of igneous-textured websterite and two-pyroxene gabbro and microgabbro of tholeiitic or calcalkalic parentage. The youngest dikes are igneous-textured clinopyroxenite, gabbro, and olivine microgabbro of alkalic parentage. The dikes in peridotite are interpreted as parts of a system of conduits through which tholeiitic (or calcalkalic) and alkalic magmas fed lower-crustal intrusions, which are represented by abundant xenoliths of the same igneous rock types as observed in the dikes. Mineral assemblages of dikes in peridotite indicate that an enriched uppermost mantle zone no thicker than 15 km could have been sampled. Because of their high densities, the gabbros and pyroxenites can occupy the zone immediately above the present Moho (modeled on seismic data as 10–13 km thick, with $V_p$ 6·8 km/s) only if their seismic velocities are reduced by the joints, partial melts, and fluid inclusions that occur in them. Alternatively, these xenoliths may have been derived entirely from beneath the Moho, in which case the Moho is not the local crust–mantle boundary.

## INTRODUCTION

The Cima volcanic field (Fig. 1) is one of many small isolated late Cenozoic basaltic volcanic fields in the Basin and Range province of the western United States. Cima lavas are dominantly hawaiite like those in some other fields (for example, western Colorado plateau volcanic fields, Best & Brimhall, 1974; Crater Flat, Nevada volcanic field, Vaniman *et al.*, 1982), but Cima differs in having abundant mafic and ultramafic xenoliths in lavas of hawaiite composition. Ultramafic xenoliths, where present in other volcanic fields, commonly occur in more primitive alkali basaltic lavas, whereas mafic xenoliths are found in lavas ranging from alkali basalt to hawaiite. The Cima xenolith assemblage gives direct evidence about the nature of magmatic additions to the region near the Moho, the creation and tapping of complex geochemical reservoirs in the upper mantle, and the mechanisms of emplacement and differentiation of basaltic magmas in the upper mantle. This paper provides basic petrologic data on this suite of mafic and ultramafic xenoliths.
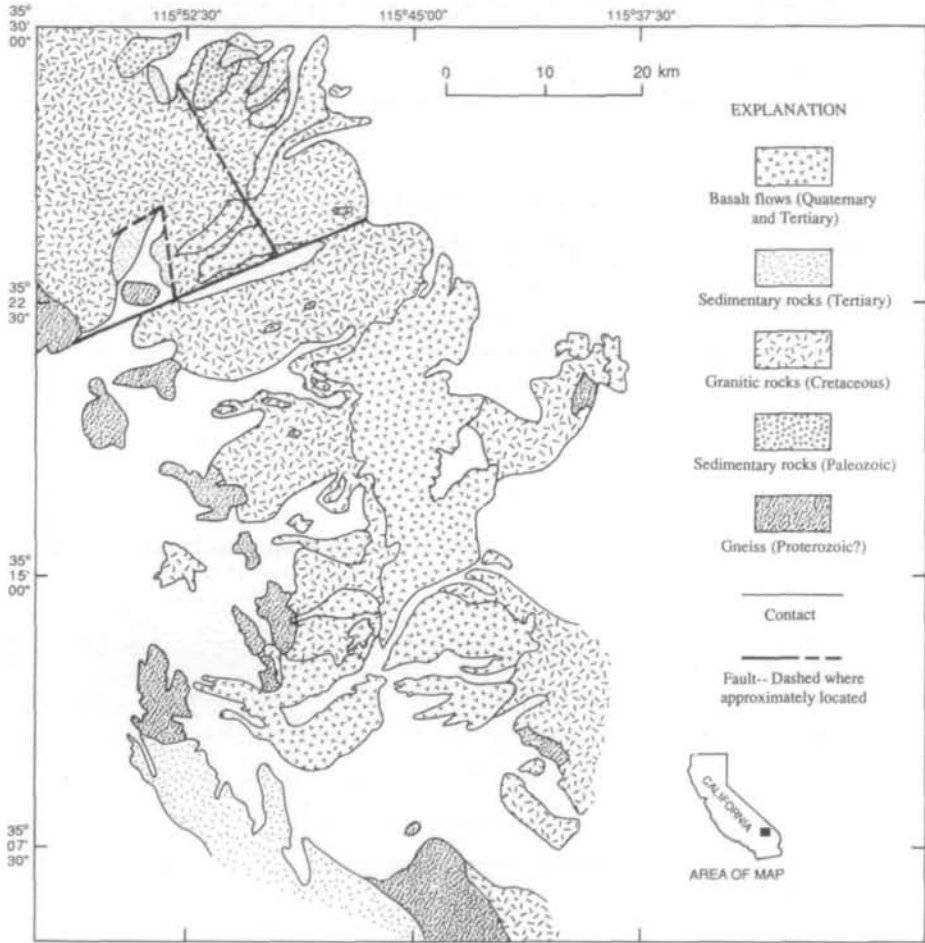
Fig. 1. Simplified geologic map of the Cima volcanic field, showing distribution of Proterozoic, Paleozoic, Cretaceous granitic, Tertiary terrigenous clastic sedimentary, and Tertiary basaltic volcanic rocks. Geology from California Division of Mines and Geology, Geologic Map of California, Kingman Sheet, 1:250 000 (1961). Identification of age of Tertiary sedimentary rocks (more extensive than shown) by Wilshire *et al.* (1987).

## GEOLOGIC SETTING

The Cima volcanic field forms the crest of the inconspicuous Ivanpah highland (Hewett, 1956; Beckerman *et al.*, 1982; Wilshire *et al.*, 1987). It is underlain by plutons of the Cretaceous Teutonia batholith and by Proterozoic gneiss, schist, and amphibolite that formed the country rock of the batholith. The Cima volcanic field occupies ~600 km$^2$ and comprises more than 50 vents and associated flows that were erupted over the last 7–8 m.y. (Turrin *et al.*, 1984). The eruptions commonly began with a maar phase where the vents encountered Tertiary gravels. The maar deposits, which contain high proportions of granitic clasts, were buried under cinders and lavas as the conduits became sealed from access to ground water. The volumes of tephra and flows from individual vents are relatively small.

The oldest volcanic rocks (~7·5 Ma) that are part of the Cima eruptive episode are of limited areal extent (Turrin *et al.*, 1984). Small remnants of 12·8-Ma trachyandesite occur within the Cima volcanic field, and are believed to be equivalent to deformed Miocene

volcanic rocks farther north in the Shadow Valley basin (Reynolds & Nance, 1988; R. E. Reynolds, pers. comm., 1989). After ~7·5 Ma, eruptive activity took place in two distinct episodes: 7·5–3 Ma and <1 Ma, with a hiatus between 3 and 1 Ma. There is no apparent systematic migration of volcanism with time (Turrin et al., 1984), and small vents that probably differ in age by half a million years coalesce.

## PETROLOGY AND COMPOSITION OF THE VOLCANIC ROCKS

The Cima volcanic rocks are dominantly ne- to hy-normative hawaiite and less abundant alkali basalt (Fig. 2; Katz & Boettcher, 1980), classified by the criteria of Vaniman et al. (1982). Microphenocrysts of olivine, plagioclase, and clinopyroxene are common, and most of the volcanic rocks contain groundmass olivine. Megacrysts of plagioclase, olivine, clinopyroxene, orthopyroxene, spinel, amphibole, and apatite are widespread in lavas and cinders. Normative values of 100 an/(an+ab) range from 29 to 54, and values of 100 Mg/(Mg+Fe$^{2+}$) (cation %) from 40 to 62; the latter are mostly well below the values (66–75) expected of magmas in equilibrium with an undepleted peridotite source rock (Irving & Price, 1981). Thus, the Cima basalts are differentiates of primitive magma, or products of mixing, or derivatives of nonperidotite sources (Wilshire, 1987).

There is no systematic relation between Mg/Fe, normative hy or ne and age (Fig. 3). However, Fig. 3 shows that a larger proportion of analyzed rocks older than 3 m.y. are hy-normative than ones younger than 1 m.y. The presence of all xenolith types is independent of all of these parameters, as is their abundance.
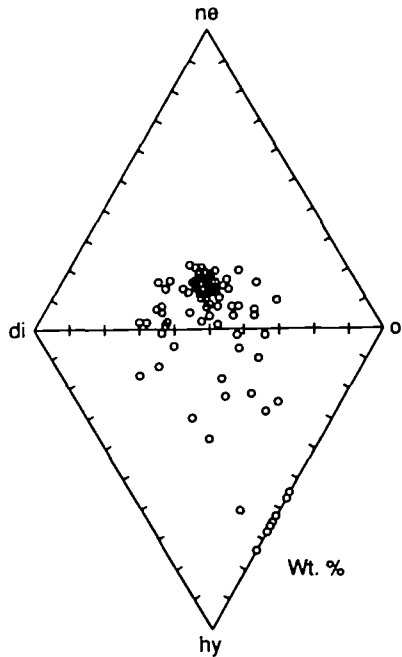


FIG. 2. Ternary plots of (CIPW) normative ne–ol–di and hy–ol–di for Cima volcanic rocks.
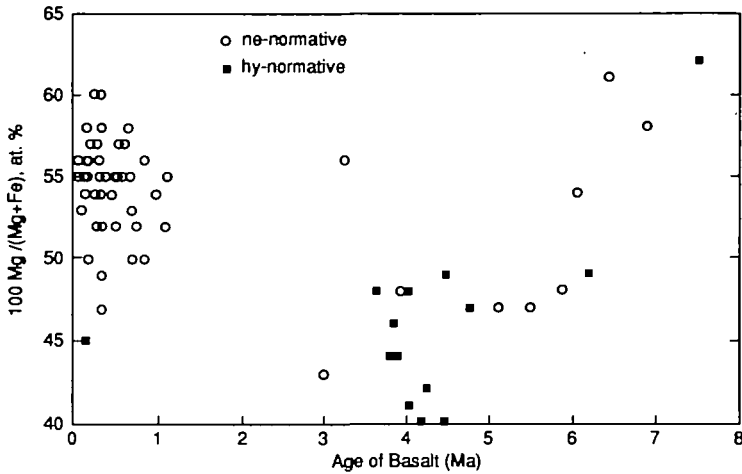
FIG. 3. Plot of 100 $Mg/(Mg+Fe^{2+})$ against age for Cima volcanic rocks.

## XENOLITHS

We divided the xenoliths into three groups based on their mineralogy: (1) Cr-diopside group of spinel peridotite and websterite; (2) green-pyroxene (not Cr-diopside) group of websterite, two-pyroxene gabbro and microgabbro; and (3) Al-augite group of clinopyroxenite, wehrlite, one-pyroxene gabbro and microgabbro. Microgabbros are identified by their small grain sizes ( $<0.5$ mm) and generally equigranular textures. Xenoliths of group 1 also commonly contain interstitial plagioclase and/or amphibole. Garnet is absent in all groups. Composite xenoliths consisting of two or more rock types of the same or different groups are unusually abundant at Cima.

### Cr-diopside group

The Cr-diopside group of xenoliths comprises peridotite and websterite. These rocks are typical of the dominant members of many basalt xenolith assemblages and consist mostly of harzburgite, lherzolite, and websterite with varying clinopyroxene/orthopyroxene ratios (Table 1). Websterite xenoliths of this group are particularly abundant at Cima. Textures of the rocks are classified according to the scheme of Pike & Schwarzman (1977), modified to include the mosaic category of Harte (1977); all are metamorphic. Essentially undeformed, allotriomorphic–granular rocks comprise 22% of the 73 samples examined in thin section; weakly to moderately deformed and recrystallized rocks with foliated, allotriomorphic–granular textures or textures transitional between allotriomorphic–granular and coarse mosaic comprise 36%; and strongly deformed and recrystallized rocks with porphyroclastic–mosaic, porphyroclastic–tabular, and tabular textures comprise 42% (see Table 9 below). Websterite generally has a coarse, mosaic texture. Pyroxenes in all of the Cr-diopside group rocks generally contain no exsolution features, and oxide contents are very low. About 25% of Cr-diopside group xenoliths contain irregularly distributed interstitial plagioclase and/or hornblende; these xenoliths and their deformed and recrystallized equivalents are described in a following section.

## TABLE 1

### Modal compositions of principal rock types among Cima xenoliths

| Sample | Ol | Opx | Cpx | Oxide | Pc | Hbl | Glass+ Xls | Rock type |
|--------|----|-----|-----|-------|----|-----|------------|-----------|
| *Cr-diopside group* | | | | | | | | |
| Ki-5-1 | 85 | 10 | 3 | 2 | | | | Harzburgite |
| Ki-5-16 | 91 | 5 | 3 | 1 | | | | Harzburgite |
| Ki-5-35 | 91 | 4 | 3 | 2 | | | | Harzburgite |
| Ki-5-82 | 88 | 8 | 2 | 2 | | | | Harzburgite |
| Ki-5-19 | 71 | 16 | 9 | 4 | tr | | | Lherzolite |
| Ki-5-52 | 80 | 7 | 10 | 3 | | | | Lherzolite |
| Ki-5-57 | 59 | 24 | 14 | 3 | | | | Lherzolite |
| Ki-5-110 | 84 | 7 | 6 | 3 | | | | Lherzolite |
| Ki-5-235 | 84 | 6 | 6 | 4 | | | | Lherzolite |
| Ki-5-1 | 16 | 32 | 44 | 8 | | | | Olivine websterite |
| Ki-5-120 | 16 | 83 | tr | | | | 1 | Websterite |
| *Green-pyroxene group* | | | | | | | | |
| Ki-5-70 | | 27 | 62 | tr | 7 | | 4 | Websterite |
| Ci-1-3 | | 45 | 41 | | 6 | | 8 | Websterite |
| Ci-1-16 | | 16 | 64 | 1 | 8 | | 11 | Websterite |
| Ci-1-20 | | 5 | 58 | tr | 26 | | 11 | Websterite |
| Ci-1-23 | | 43 | 40 | 1 | 14 | | 3 | Websterite |
| Ci-1-57 | | 52 | 16 | tr | 13 | | 19 | Websterite |
| Ci-1-64 | | 47 | 44 | 1 | 4 | | 4 | Websterite |
| Ci-9-7 | | 41 | 59 | | | | | Websterite - |
| Ci-1-160 | 45 | 11 | 33 | tr | 5 | tr | 6 | Olivine websterite |
| Ci-1-163 | 2 | 33 | 48 | | 10 | | 7 | Olivine websterite |
| Ci-1-165 | 31 | 15 | 28 | | 18 | | 8 | Olivine websterite |
| Ci-6-2 | 41 | 4 | 20 | tr | 35 | | tr | Troctolite* |
| Ki-5-18 | | 15 | 23 | | 41 | | 21 | Gabbro |
| Ki-5-30 | | 23 | 37 | | 37 | | 3 | Gabbro |
| Ki-5-47 | | 10 | 26 | | 53 | | 11 | Gabbro |
| Ci-1-2 | | 1 | 28 | 1 | 48 | | 22 | Gabbro |
| Ki-5-40 | 4 | 4 | 39 | 2 | 47 | | 4 | Olivine gabbro |
| Ki-5-42 | | 12 | 30 | tr | 55 | | 3 | Gabbro |
| Ki-5-112 | | 18 | 32 | | 33 | | 17 | Gabbro |
| Ci-1-1 | | tr | 46 | 4 | 36 | | 14 | Gabbro |
| Ci-1-265 | | 15 | 17 | | 61 | | 7 | Gabbro |
| Ci-1-2 | | 24 | 28 | | 48 | | | Microgabbro |
| Ki-5-91 | 4 | 15 | 30 | 5 | 46 | | | Microgabbro |
| *Al-augite group* | | | | | | | | |
| Ki-2-10 | 1 | | 67 | 16 | 9 | | 7 | Clinopyroxenite |
| Ki-2-103 | | | 87 | 11 | tr | tr | 2 | Clinopyroxenite |
| Ki-2-9 | | | 84 | 13 | | tr | 2 | Clinopyroxenite |
| Ki-2-12 | 1 | | 68 | 10 | 2 | | 19 | Clinopyroxenite |
| Ki-2-26 | tr | | 79 | 15 | 1 | tr | 5 | Clinopyroxenite |
| Ci-9-80 | | | 75 | 21 | 1 | | 3 | Clinopyroxenite |
| Ci-9-108 | | | 55 | 18 | 2 | | 25 | Clinopyroxenite |
| Ci-9-100 | | | 77 | 15 | | | 8 | Clinopyroxenite |
| Ki-2-28 | 4 | | 55 | 15 | 23 | | 3 | Gabbro |
| Ki-5-97 | 11 | | 35 | tr | 43 | | 10 | Gabbro |
| Ci-1-102 | | | 47 | 4 | 34 | | 21 | Gabbro |
| Ki-5-88 | 5 | | 29 | 9 | 35 | | 22 | Microgabbro |
| Ki-5-241 | 11 | | 26 | 5 | 35 | | 23 | Microgabbro |
| *Two-pyroxene subgroup, Al-augite group* | | | | | | | | |
| Ki-5-200 | 2 | 8 | 38 | 3 | 3 | | 46 | Websterite† |
| Ci-1-354 | | 1 | 55 | 1 | | tr | 43 | Websterite† |
| Ci-1-381 | | 5 | 41 | 2 | | | 52 | Websterite† |

\* Pyroxenes present dominantly as small lithic clasts (xenoliths).
† Orthopyroxene selectively melted.

## Green-pyroxene group

Members of the green-pyroxene group are distinguishable in hand specimen from Cr-diopside websterites by the duller color of clinopyroxene and by the common euhedral projections of pyroxenes into interstitial plagioclase. They are distinguishable from most members of the Al-augite group by the color of clinopyroxene and by the generally abundant orthopyroxene in the former. Green-pyroxene group xenoliths are fine- to coarse-grained igneous rocks that only rarely (three of 61 samples examined in thin section) show any sign of solid-state deformation and local recrystallization. They are substantially more abundant than xenoliths of the Al-augite group in the volcanic field as a whole, but not in all individual localities. Dominant rock types are websterite and two-pyroxene gabbro (Table 1). Two-pyroxene microgabbro is less abundant, as are clinopyroxenite, orthopyroxenite, troctolite, and anorthosite. Hornblendites may be members of this group or of the Al-augite group or both.

Two types of websterite are recognized on the basis of modal composition: olivine websterite, which appears to be modally gradational to olivine gabbro and troctolite; and olivine-free websterite, which is modally gradational to two-pyroxene gabbro. Clinopyroxene–orthopyroxene ratios and proportions of plagioclase in both types are extremely variable, as are pyroxene ratios in gabbros. Among the 30 two-pyroxene gabbros examined in thin section, olivine is a primary mineral (as opposed to quench crystals in glass) in five, and amphibole is an essential mineral in two. With few exceptions, primary oxide minerals (see Table 1) are scarce in all rock types of this group. In a few samples, opaque minerals occur in clusters of small grains partly or wholly enclosed in plagioclase (Fig. 4a) or, rarely, in orthopyroxene.

A distinctive feature of this group of rocks is well-developed blebby and lamellar exsolution in both pyroxenes. In addition, the internal textures of the pyroxenes commonly are complex. The clinopyroxenes may have what is here called 'patchwork' texture in which grains comparable in size to typical grains in the rock are composed of complex intergrowths of clinopyroxenes with markedly different orientations (Fig. 4b). These patches or whole grains may also comprise symplectic intergrowths of clinopyroxene and orthopyroxene (Fig. 4b). Growth twins in one clinopyroxene in a patchwork grain may be crossed by optically continuous, untwinned patches with different orientation (Fig. 4c). Rims of clinopyroxene with no symplectic orthopyroxene are common; these rims may extend interstitially around several grains, including minerals other than clinopyroxene, or pass through as well as around clusters of pyroxene symplectite (Fig. 4d). Some clinopyroxenes, especially those in mafic members of the group, have brown amphibole lamellae or oriented inclusions of amphibole with irregular shapes. Some xenoliths contain apparently single pyroxene grains that are 'half-and-half' orthopyroxene and clinopyroxene with complex boundaries (Fig. 4e). Textures of this sort are found in xenoliths elsewhere in the world, e.g., Hualalai, Hawaii (Bohrson & Clague, 1988) and in the San Francisco volcanic field, Arizona (Wilshire et al., 1988), but do not to our knowledge occur in high-level crustal intrusions.

Dominant textures in rocks of the green-pyroxene group are hypidiomorphic–granular equigranular, but allotriomorphic–granular poikilitic, and equigranular–polygonal textures also occur. Igneous lamination is rare. In poikilitic rocks, plagioclase is the dominant oikocryst phase, but clinopyroxene and amphibole may also play this role in the same or different xenoliths. Mineral grains enclosed in oikocrysts are generally euhedral to subhedral, but more complex intergrowths also occur (Fig. 4f–h). Equigranular–polygonal textures are found in orthopyroxene-rich members of this group (Fig. 5a).

Two-pyroxene microgabbros are not abundant. Textures range from trachytic equigranular to fine-grained granular. Many of these rocks contain megacrysts (1–2 mm) of ortho-

pyroxene, and small (three or four grains) lithic clasts consisting of clinopyroxene and/or orthopyroxene grains. In olivine-bearing two-pyroxene microgabbros, spongy olivine oikocrysts partly enclose small plagioclase grains.

Compositional zoning of minerals in rocks of the green-pyroxene group is common but rarely pronounced. Both pyroxenes generally are zoned with exsolved cores surrounded by thin rims free of exsolved phases. Plagioclase in the mafic rocks may be unzoned, but in gabbro it commonly shows patchy normal zoning, or, less commonly, normal oscillatory zoning with six or fewer oscillations.

The order of appearance of phases deduced from textural relations is:

(1)  olivine websterite: olivine–orthopyroxene–clinopyroxene–plagioclase–oxide;
(2)  olivine-free websterite: orthopyroxene–clinopyroxene–plagioclase + amphibole–oxide;
(3)  gabbro: either orthopyroxene–plagioclase–clinopyroxene + amphibole–oxide, or plagioclase–orthopyroxene–clinopyroxene–oxide.

There are, however, a number of ambiguities in the textural relations: in olivine websterites, olivine forms anhedra enclosed in orthopyroxene, but also occurs as euhedra enclosed in or intergrown with late interstitial plagioclase. In some rocks, for example the troctolites, in which these same textural relations of olivine occur, the pyroxene-rounded olivine aggregates form clusters in the troctolite. These relations may result from inclusion of olivine xenocrysts and lithic fragments in melts from which olivine continued to crystallize, or from crystallization of partial melts of olivine websterite (Wilshire, 1988). The patchwork clinopyroxenes also are of uncertain origin; they may be inclusions of early-formed or xenocrystal clinopyroxene in later pyroxene, complex intergrowths of simultaneously crystallized pyroxenes, or of some other origin. The amoeboid inclusions of one mineral in another (Fig. 4f–h) may reflect substantial overlap in time of crystallization of both phases, differences in cooling rates, or other causes. Although the origin of these textures is not understood, it is important to recognize that they are not the types of features found in exposed stratiform basaltic intrusions in the crust.

## Al-augite group

Members of the Al-augite group are fine- to very coarse-grained (pegmatitic) rocks that are believed to be mostly igneous, although textures of pyroxenite members commonly are ambiguous. Dominant lithologies are clinopyroxenite, one-pyroxene gabbro, and olivine microgabbro (Table 1).

A poorly represented subgroup comprises websterites and two-pyroxene gabbros, some of which have pyroxene exsolution features resembling those of the green-pyroxene group; these rocks are distinguished from the green-pyroxene group in having more Fe-rich pyroxenes and in being ne-normative. Rocks of this subgroup at Cima also show high degrees of melting (Table 1) although abundant little-melted xenoliths of the same type occur at other localities (Wilshire, 1990). Hornblendites, and less common glimmerites, may be derivatives of either green-pyroxene or Al-augite group magmas. Wehrlites are uncommon, and a small group of websterites share characteristic features of the green-pyroxene and Al-augite groups. A single biotite clinopyroxenite xenolith is assigned to the Al-augite group.

Distinctive features of this group are general absence or very weak development of orthopyroxene exsolution in clinopyroxene, abundant oxides (mostly pleonaste), and the presence of only trace amounts, if any, of orthopyroxene, with the exception of the websterites and gabbros mentioned above. Modal gradations exist from clinopyroxenite to
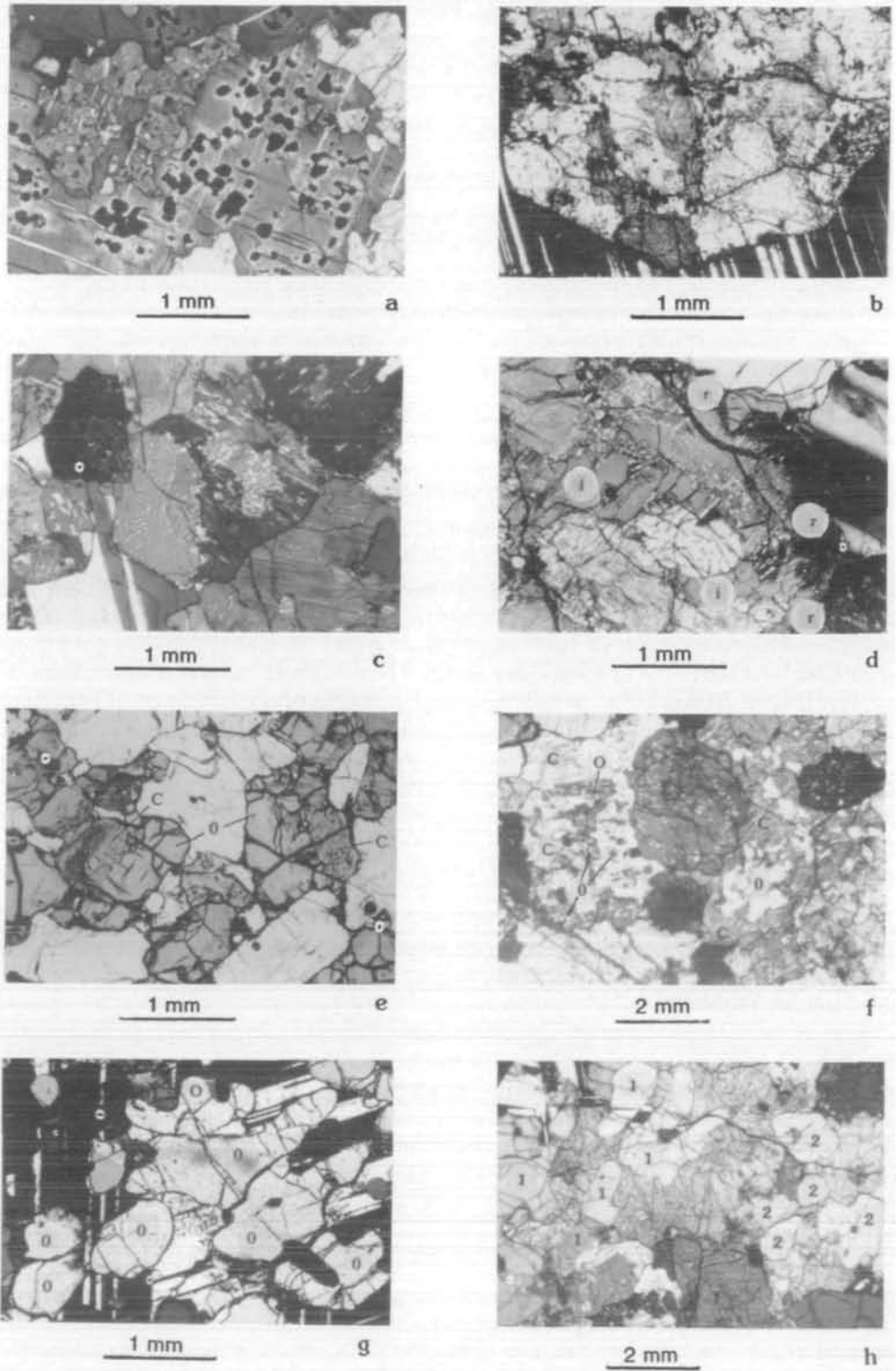
Fig. 4

gabbro. Of 36 samples examined in thin section, hornblende occurs in three clinopyroxenites and biotite in one. Olivine is a primary mineral in three clinopyroxenites and five gabbros. Plagioclase occurs as an interstitial mineral in a few clinopyroxenites but is more common as coronas on spinel, where it is generally intergrown with subhedral olivine. The coronal relation is very irregularly distributed through the clinopyroxenites, even within a single thin section.

The most common texture of pyroxenite members of the Al-augite group is allotrio-morphic–granular inequigranular, but some have hypidiomorphic–granular textures. The clinopyroxenes are intergrown with spinel of the same textural habit in many rocks, but in the same or different rocks, small euhedral to subhedral spinels are enclosed in clinopyroxene; and in some, the spinel forms hollyleaf textures as a consequence of molding on pyroxene grains.

Microgabbros of the Al-augite group are mostly poikilitic rocks with equidimensional plagioclase and clinopyroxene grains enclosed in open-textured olivine oikocrysts in which optically continuous parts of olivine grains are not visibly connected. Clinopyroxenes, commonly sieved with glass, are interstitial to plagioclase. A common texture is large pyroxene-free patches of small equidimensional plagioclase grains partly enclosed by olivine oikocrysts. Most of the microgabbros are holocrystalline but some contain interstitial glass, and a few contain large amounts of glass.

Olivine, where present, was the first phase to crystallize in olivine pyroxenites, wehrlites, and gabbros, but one of the last to crystallize in microgabbros. Plagioclase probably followed olivine in gabbros and overlapped crystallization of clinopyroxene. Crystallization of oxides appears to have overlapped and followed clinopyroxene.

## BULK CHEMICAL COMPOSITION OF XENOLITHS

One hundred and six xenoliths representing all the principal rock types and many of the minor rock types have been analyzed for major element composition by X-ray fluorescence (XRF) with gravimetric analysis of FeO, $H_2O$, and $CO_2$. Representative compositions for the main rock types are shown in Table 2. A full data set is available on request. All of the many variation diagrams plotted show a great deal of scatter, particularly for elements of <1% concentration. Because of its broad range of values, MgO (wt.%) was chosen to illustrate variability of other oxide weight percentages in representative rock types (Figs. 6–9). The following description of compositional variations is organized to facilitate comparison of similar rock types from different groups as well as intragroup trends.

FIG. 4. Photomicrographs of Cima xenoliths. (a) Clusters of opaque minerals enclosed in plagioclase in two-pyroxene gabbro. Cause of light halos around opaque grains is not known. Crossed polarizers. (b) Patchwork texture in clinopyroxene, showing irregular shapes of differently oriented subgrains, some of which are symplectic intergrowths with orthopyroxene. Crossed polarizers. (c) Clinopyroxene patch across growth twin (diagonal, dipping right in upper part of central clinopyroxene grain) in host clinopyroxene. Crossed polarizers. (d) Exsolution-free clinopyroxene rim (r) around cluster of symplectic grains also extends into the cluster (i). The outer part of the rim is zoned and exposes crystal faces to surrounding grains, but it has subsequently been partly melted. Crossed polarizers. (e) Pyroxene grains, of overall size comparable to the size of surrounding minerals, composed of about equal parts of clinopyroxene (C) and orthopyroxene (O) joined along complex boundaries. Plane-polarized light. (f) Two highly irregular, 'amoeboid' inclusions of orthopyroxene (O) in two clinopyroxene grains (C). Crossed polarizers. (g) 'Amoeboid' olivine (O designates optically continuous olivines) intergrown with plagioclase. Crossed polarizers. (h) Two 'amoeboid' olivine grains (1, 2) partly enclosed by symplectic clinopyroxene grains; note olivine grain (two top left segments) crosses interstitial plagioclase separating two clinopyroxene grains. Crossed polarizers.
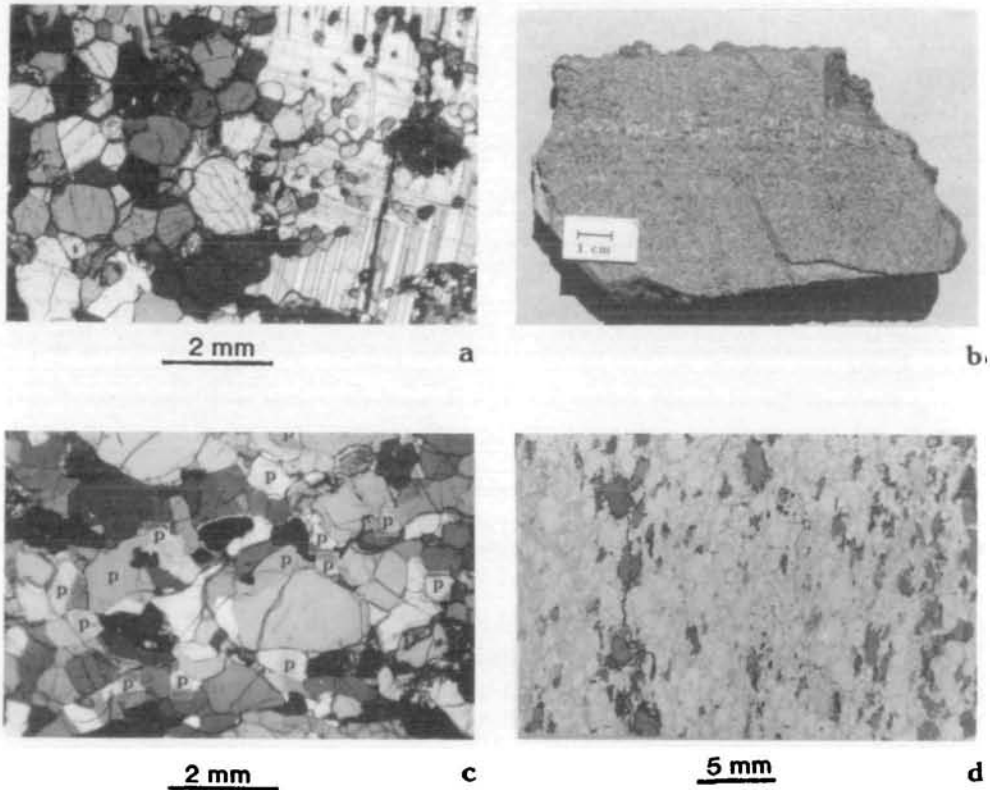
FIG. 5. Photomicrographs and cut-slab photographs of Cima xenoliths. (a) Equigranular mosaic of orthopyroxene grains in composite green-pyroxene orthopyroxenite–gabbro. Interstitial clinopyroxene and plagioclase in orthopyroxenite are locally molded on the orthopyroxenes, but where absent, the orthopyroxenes have triple-junction boundaries. The orthopyroxene grains contain thin clinopyroxene exsolution lamellae. Crossed polarizers. (b) Cut slab showing grain-boundary infiltration of melt from which plagioclase crystallized, controlled by a now-healed fracture in Cr-diopside websterite. (c) Penetratively deformed and recrystallized Cr-diopside peridotite. Infiltration by melt from which plagioclase crystallized occurred before deformation and recrystallization, and the plagioclase (P) is now in textural equilibrium with the peridotite. Crossed polarizers. (d) Penetratively deformed and recrystallized Cr-diopside peridotite. Infiltration by melt from which amphibole crystallized occurred before deformation and recrystallization, and the amphibole (dark grains) is now in textural equilibrium with the peridotite. The amphibole grains are marginally melted, probably because of entrainment in the host basalt. Plane-polarized light.

## Peridotite

Figure 6 plots major elements vs. MgO for three kinds of peridotite: refractory magnesian Cr-diopside spinel peridotite; reacted Cr-diopside peridotite adjacent to dikes; and Cr-diopside peridotite containing interstitial plagioclase, pyroxene, and amphiboles ('infiltrated' peridotite). Reacted peridotites are identified by more Fe-rich compositions in the silicate phases and more aluminous compositions in the spinel (Wilshire et al., 1988). The magnesian peridotites show only a small range of MgO (mostly 42–47), but substantial ranges in Al, Mg, Ca, and Na (and Si, not shown in Fig. 6), which reflect the modal variations of the analyzed rocks. Reacted peridotites show a wide range of MgO (32–42), and Fe, Ti enrichment at the expense of Si and Mg. Such enrichment is typical of peridotites in reaction zones of dikes and other xenoliths regarded as representative of 'fertile mantle' and 'primitive asthenosphere' compared with common magnesian peridotites (see Wilshire et al., 1988, table 5). The infiltrated peridotites extend the range of MgO of reacted peridotites. The
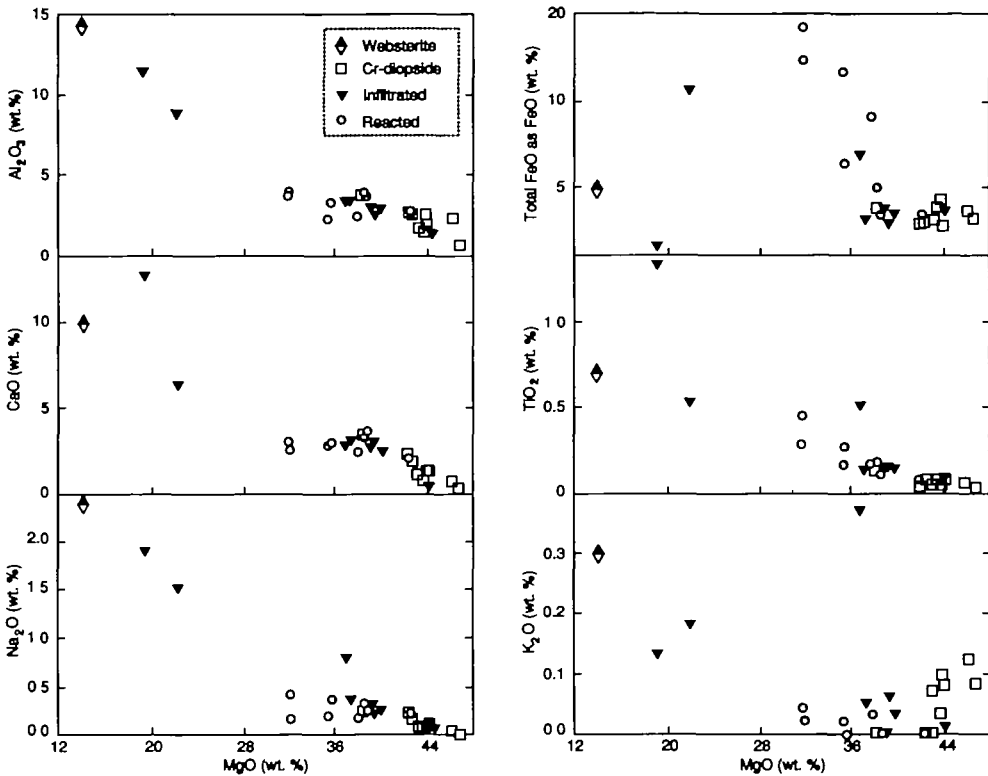
FIG. 6. Variation of major elements in Cr-diopside, infiltrated, and reacted peridotites with respect to MgO.

extent of enrichment of Al, Ca, Na, K, and Ti in infiltrated peridotite compared with magnesian peridotite is directly related to the proportion of interstitial plagioclase, pyroxene, and amphibole; the least enriched rocks are peridotite with a few per cent of interstitial plagioclase. Of the most enriched rocks in Fig. 6, two are infiltrated shear zones consisting of angular lithic and mineral debris cemented by introduced plagioclase, pyroxene, and amphibole (one in peridotite and one in Cr-diopside websterite); and one is peridotite impregnated by amphibole and plagioclase adjacent to a feldspathic hornblende pyroxenite dike. At the other end of the spectrum, there are varying degrees of contamination of dike rocks by crystal and lithic debris derived from the Cr-diopside peridotite wallrock.

## Pyroxenite

Figure 7 illustrates chemical variation with respect to MgO among Cr-diopside websterites, green-pyroxene pyroxenites, Al-augite websterites, and Al-augite clinopyroxenites. These groups are separable, with some overlap, as shown in Fig. 7, except that the two Al-augite types occupy similar fields. Most members of the Al-augite group form an isolated cluster for Al (and Si, not shown in Fig. 7), reflecting the abundance of aluminous spinel (Table 1), whereas Cr-diopside and green-pyroxene pyroxenites, both dominantly websterite, show wide ranges of MgO and roughly parallel trends for most oxides; these trends reflect varying proportions of orthopyroxene and clinopyroxene, and, in the green-pyroxene

TABLE 2

Bulk chemical compositions and CIPW norms for Cima xenoliths

| Rock type | Cr-diopside peridotite | | | | Cr-diopside websterite | | Green-pyroxene websterite | | | | | Green-pyroxene olivine websterite | | Al-augite clinopyroxenite | |
|---|---|---|---|---|---|---|---|---|---|---|---|---|---|---|---|
| Sample no. | Ki-5-16 | Ki-5-19 | Ki-5 57 | Ki-5 110 | Ki-5-1 | Ki-5-120 | Ci-1-3 | Ci-1-16 | Ci-1-23 | Ci-1-64 | Ci-9-84 | Ci-1-160 | Ci-1-163 | Ci-1-165 | Ci-9-80 |
| $SiO_2$ | 42·50 | 45·20 | 44·90 | 44·30 | 46·70 | 51·90 | 52·30 | 49·70 | 51·90 | 52·90 | 50·60 | 45·50 | 48·70 | 46·80 | 39·90 |
| $Al_2O_3$ | 0·68 | 3·83 | 2·54 | 1·90 | 6·60 | 4·20 | 5·36 | 7·73 | 6·00 | 5·86 | 5·48 | 3·75 | 7·27 | 6·46 | 16·60 |
| $Fe_2O_3$ | 0·53 | 1·26 | 1·10 | 0·36 | 1·70 | 2·10 | 2·20 | 2·64 | 2·10 | 2·30 | 3·02 | 1·48 | 1·84 | 1·39 | 6·40 |
| FeO | 7·70 | 7·68 | 6·87 | 7·40 | 5·00 | 4·80 | 10·07 | 6·38 | 9·57 | 9·76 | 4·44 | 9·83 | 7·88 | 11·44 | 3·81 |
| MgO | 46·90 | 38·30 | 42·60 | 44·10 | 33·00 | 18·90 | 23·60 | 14·50 | 22·80 | 23·40 | 16·20 | 29·00 | 17·70 | 21·50 | 14·00 |
| CaO | 0·40 | 3·50 | 2·05 | 1·50 | 5·70 | 15·90 | 5·24 | 16·10 | 5·45 | 4·22 | 18·50 | 7·44 | 12·20 | 8·22 | 16·80 |
| $Na_2O$ | — | 0·26 | 0·17 | 0·10 | 0·28 | 0·61 | 0·61 | 1·18 | 0·80 | 0·73 | 0·75 | 0·75 | 1·00 | 1·30 | 0·67 |
| $K_2O$ | 0·08 | — | — | 0·08 | 0·12 | 0·05 | 0·05 | 0·08 | 0·04 | 0·19 | 0·05 | — | 0·14 | 0·18 | 0·07 |
| $H_2O$ | 1·10 | 0·03 | 0·07 | 0·07 | 0·35 | 0·43 | 0·11 | 0·17 | 0·19 | 0·19 | 0·70 | 0·12 | 0·21 | 0·21 | 0·76 |
| $TiO_2$ | 0·02 | 0·13 | 0·06 | 0·06 | 0·15 | 0·40 | 0·60 | 1·47 | 1·37 | 0·69 | 0·60 | 0·68 | 1·32 | 1·02 | 1·34 |
| $P_2O_5$ | 0·04 | — | — | 0·04 | — | 0·14 | — | — | — | 0·09 | — | 0·04 | 0·08 | 0·06 | — |
| MnO | 0·12 | 0·15 | 0·13 | 0·11 | 0·07 | 0·16 | 0·21 | 0·16 | 0·19 | 0·20 | 0·17 | 0·17 | 0·16 | 0·19 | 0·16 |
| Total | 100·07 | 100·34 | 100·49 | 100·02 | 99·67 | 99·59 | 100·35 | 100·11 | 100·74 | 100·53 | 100·51 | 98·76 | 98·50 | 98·77 | 100·51 |
| q | — | — | — | — | — | — | — | — | — | — | — | — | — | — | — |
| or | 0·5 | — | — | 0·5 | 0·7 | 0·3 | 0·3 | 0·5 | 0·2 | 1·1 | 0·3 | — | 0·8 | 1·1 | — |
| ab | — | 2·2 | 1·4 | 0·8 | 2·4 | 5·2 | 5·1 | 9·9 | 6·7 | 6·1 | 6·3 | 6·4 | 8·6 | 11·1 | — |
| an | 1·6 | 9·2 | 6·1 | 4·5 | 16·4 | 8·6 | 11·7 | 15·5 | 12·6 | 12·1 | 11·4 | 7·0 | 15·2 | 11·4 | 41·7 |
| ne | — | — | — | — | — | — | — | — | — | — | — | — | — | — | 3·0 |
| wo | — | 3·3 | 1·6 | 1·1 | 4·9 | 29·1 | 5·5 | 25·7 | 5·7 | 3·0 | 32·7 | 12·6 | 1 | 12·3 | 10·9 |
| en | 10·3 | 19·4 | 18·3 | 15·2 | 27·2 | 41·9 | 53·3 | 28·6 | 51·9 | 55·9 | 32·9 | 18·8 | 29·8 | 19·2 | 9·4 |
| fs | 1·2 | 2·7 | 2·0 | 1·9 | 2·5 | 6·0 | 14·6 | 5·9 | 12·7 | 14·6 | 4·1 | 4·2 | 7·5 | 6·6 | — |
| fo | 74·6 | 53·0 | 61·1 | 66·3 | 38·7 | 3·7 | 3·6 | 5·1 | 3·2 | 1·4 | 5·0 | 38·1 | 10·5 | 24·6 | 17·6 |
| fa | 9·8 | 8·0 | 7·5 | 8·9 | 4·0 | 0·6 | 1·1 | 1·2 | 0·9 | 0·4 | 0·7 | 9·3 | 2·9 | 9·4 | — |
| cs | — | — | — | — | — | — | — | — | — | — | — | — | — | — | 3·6 |
| mt | 0·8 | 1·8 | 1·6 | 0·5 | 2·5 | 3·1 | 3·2 | 3·8 | 3·0 | 3·3 | 4·3 | 2·2 | 2·7 | 2·0 | 8·8 |
| il | — | 0·2 | 0·1 | 0·1 | 0·3 | 0·8 | 1·1 | 2·8 | 2·6 | 1·3 | 1·1 | 1·3 | 2·5 | 2·0 | 2·5 |
| ap | 0·1 | — | — | 0·1 | — | 0·3 | — | — | — | 0·2 | — | 0·1 | 0·2 | 0·1 | — |

TABLE 2 (*Continued*)

| Rock type | Al-augite clinopyroxenite | | | Al-augite websterite | | Green-pyroxene gabbro | | | | Al-augite gabbro | | Green-pyroxene microgabbro | | Al-augite microgabbro | |
|---|---|---|---|---|---|---|---|---|---|---|---|---|---|---|---|
| Sample no. | Ci-9-100 | Ci-9-108 | K-5-200 | Ci-1-354 | Ci-1-381 | Ki-5-47 | Ci-1-2 | Ci-6-2A* | Ci-6-2B* | Ki-2-28 | Ci-1-102 | Ci-1-2 | Ki-5-91 | Ki-5-88 | Ki-5-241 |
| $SiO_2$ | 41·40 | 40·70 | 44·20 | 46·70 | 47·30 | 51·50 | 50·70 | 44·50 | 43·30 | 42·87 | 46·50 | 52·20 | 47·20 | 42·80 | 47·30 |
| $Al_2O_3$ | 15·50 | 16·60 | 10·30 | 9·69 | 9·48 | 16·50 | 17·80 | 7·89 | 8·92 | 20·16 | 13·00 | 14·70 | 12·50 | 13·10 | 14·50 |
| $Fe_2O_3$ | 5·52 | 5·37 | 4·60 | 3·36 | 3·44 | 1·30 | 5·06 | 1·30 | 0·32 | 4·70 | 3·96 | 3·65 | 5·70 | 8·10 | 4·30 |
| $FeO$ | 3·73 | 3·64 | 7·40 | 6·61 | 5·72 | 6·50 | 1·90 | 12·54 | 13·39 | 3·38 | 7·06 | 3·33 | 8·70 | 9·10 | 7·60 |
| $MgO$ | 14·80 | 14·80 | 14·80 | 14·40 | 15·30 | 7·80 | 7·44 | 26·40 | 26·40 | 10·23 | 9·43 | 11·40 | 11·70 | 9·53 | 8·85 |
| $CaO$ | 17·30 | 16·50 | 14·90 | 16·20 | 16·90 | 11·00 | 12·90 | 5·94 | 4·34 | 15·95 | 14·00 | 11·70 | 9·40 | 11·90 | 11·20 |
| $Na_2O$ | 0·62 | 0·68 | 0·98 | 1·52 | 1·12 | 2·70 | 3·02 | 1·23 | 1·50 | 1·36 | 2·01 | 2·44 | 2·10 | 1·99 | 2·72 |
| $K_2O$ | 0·03 | 0·12 | 0·13 | 0·14 | 0·20 | 0·26 | 0·37 | 0·08 | 0·06 | 0·10 | 0·27 | 0·13 | 0·12 | 0·17 | 0·25 |
| $H_2O$ | 0·61 | 1·19 | 0·21 | 0·15 | 0·12 | 0·83 | 0·14 | 0·09 | 0·08 | 0·10 | 0·26 | 0·13 | 0·62 | 0·37 | 0·35 |
| $TiO_2$ | 1·20 | 1·18 | 1·90 | 1·39 | 1·02 | 0·96 | 0·92 | 0·34 | 0·18 | 1·09 | 3·54 | 0·53 | 1·20 | 2·21 | 2·35 |
| $P_2O_5$ | — | — | 0·08 | 0·18 | 0·10 | 0·14 | 0·07 | — | — | 0·04 | 0·10 | — | 0·09 | 0·07 | 0·09 |
| $MnO$ | 0·16 | 0·14 | 0·19 | 0·18 | 0·17 | 0·13 | 0·10 | 0·16 | 0·16 | 0·12 | 0·15 | 0·11 | 0·20 | 0·14 | 0·17 |
| Total | 100·87 | 100·92 | 99·69 | 100·52 | 100·87 | 99·62 | 100·42 | 100·47 | 98·65 | 100·10 | 100·28 | 100·32 | 99·53 | 99·48 | 99·68 |
| q | — | — | — | — | — | 0·7 | tr | — | — | — | — | 0·8 | — | — | — |
| or | — | — | 0·8 | 2·4 | 1·2 | 1·5 | 2·2 | 0·5 | 0·4 | 0·6 | 1·6 | 0·8 | 0·7 | 1·0 | 1·5 |
| ab | — | — | 7·0 | 4·9 | 5·4 | 22·9 | 25·4 | 10·4 | 12·9 | 2·9 | 16·9 | 20·6 | 17·8 | 16·9 | 23·1 |
| an | 39·0 | 41·5 | 23·4 | 18·2 | 20·1 | 32·2 | 33·7 | 15·7 | 17·7 | 48·5 | 25·6 | 28·6 | 24·4 | 26·4 | 26·7 |
| ne | 2·8 | 3·1 | 0·7 | 4·3 | 2·2 | — | — | — | — | 4·7 | — | — | — | — | — |
| wo | 13·5 | 10·6 | 20·5 | 25·0 | 25·9 | 3·3 | 11·4 | 5·7 | 1·7 | 12·5 | 17·7 | 11·8 | 8·7 | 12·9 | 11·2 |
| en | 11·5 | 9·0 | 15·5 | 18·7 | 19·9 | 19·5 | 18·4 | 7·1 | 1·9 | 10·6 | 16·3 | 28·3 | 23·1 | 10·9 | 13·6 |
| fs | 0·2 | 0·1 | 2·9 | 3·9 | 3·3 | 9·5 | — | 2·3 | 0·7 | 0·3 | 2·9 | 2·4 | 7·6 | 3·0 | 4·3 |
| fo | 17·5 | 19·3 | 15·0 | 11·8 | 12·5 | — | — | 40·9 | 45·4 | 10·4 | 5·0 | — | 4·3 | 9·1 | 6·0 |
| fa | 0·3 | 0·3 | 3·1 | 2·7 | 2·3 | — | — | 14·9 | 18·5 | 0·3 | 1·0 | — | 1·6 | 2·8 | 2·1 |
| cs | 3·8 | 4·4 | — | — | — | — | — | — | — | — | — | — | — | — | — |
| mt | 7·9 | 7·7 | 6·7 | 4·8 | 4·9 | 1·9 | 3·8 | 1·9 | 0·5 | 6·8 | 5·7 | 5·3 | 8·3 | 11·8 | 6·2 |
| il | 2·3 | 2·2 | 3·6 | 2·6 | 1·9 | 1·8 | 1·7 | 0·6 | 0·3 | 2·1 | 6·7 | 1·0 | 2·3 | 4·2 | 4·3 |
| ap | — | — | 0·2 | 0·4 | 0·2 | 0·3 | 0·2 | — | — | 0·1 | 0·2 | — | 0·2 | 0·2 | 0·2 |

\* Ci-6-2A, whole rock; Ci-6-2B px clusters (websterite xenoliths) removed.

Analysts, XRF: J. Taggart, A. Bartel, D. Siems, L. Espos, U.S. Geological Survey; FeO, $H_2O$, $CO_2$: T. Fries, N. Elsheimer, L. Espos, S. Neil.
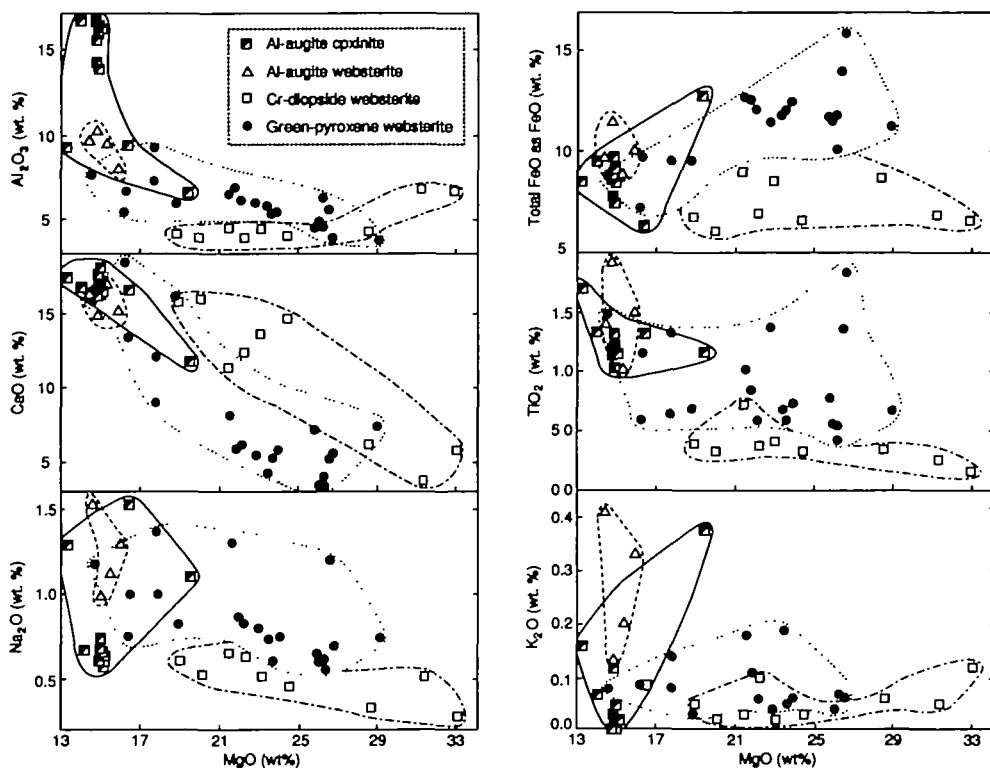
FIG. 7. Variation of major elements in Cr-diopside, green-pyroxene, and Al-augite pyroxenites with respect to MgO.

group, abundance of olivine. Low and high Fe subgroups of the green-pyroxene pyroxenites are olivine websterite and olivine-free websterite respectively.

### Gabbro and microgabbro

Gabbros and microgabbros of the green-pyroxene and Al-augite groups show nearly complete overlap of MgO. All oxides show wide scatter and little or no systematic variation with MgO.

### Green-pyroxene and Al-augite groups

Figures 8 and 9 illustrate within-group variations for the green-pyroxene and Al-augite groups. Despite substantial scatter, there are systematic large increases in Al, Na, and K with decreasing MgO from green-pyroxene group pyroxenites through gabbro; microgabbro covers the full range covered by gabbro. The trend of Ti (and weak trend of Fe) in Fig. 8 is skewed by a single gabbro that contains an unusual abundance of Fe, Ti oxides.

In contrast, members of the Al-augite group show more scatter (Fig. 9) and a bimodal separation into a high-MgO group containing all the pyroxenites and some gabbros and a low-MgO group of gabbro and microgabbro with high Fe, Na, K, and Ti, and low Mg and Ca.
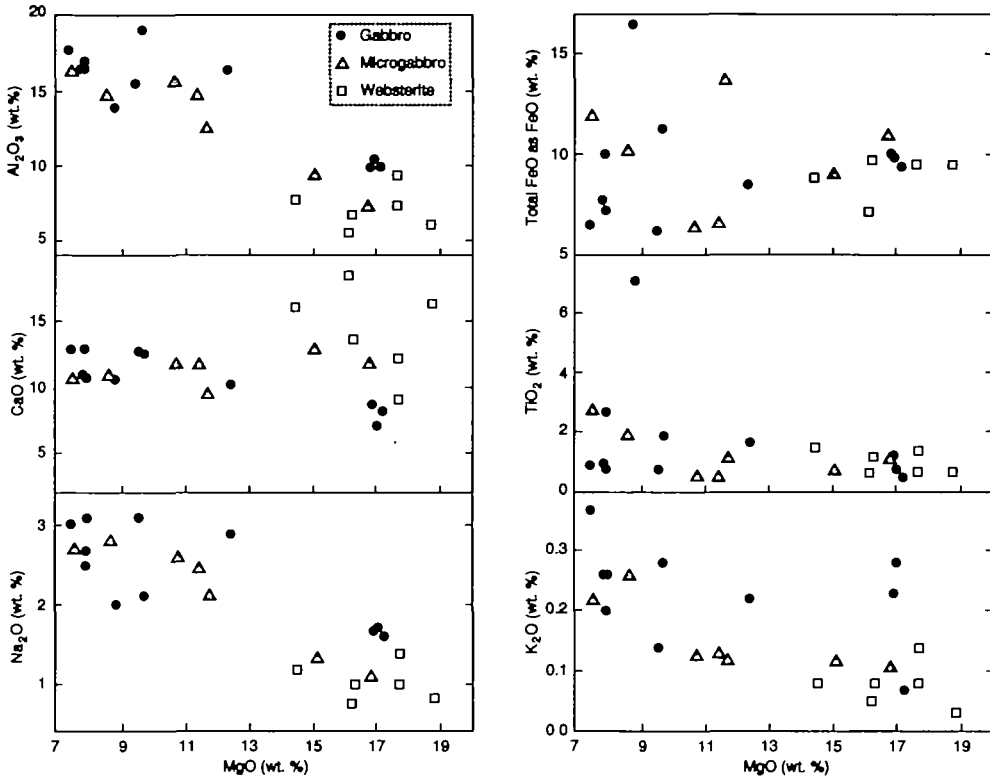
FIG. 8. Variation of major elements in rocks of the green-pyroxene group with respect to MgO.

## MINERAL COMPOSITIONS

### Analytical methods

Mineral analyses were done at the U.S. Geological Survey with an ARL SEMQ automated electron microprobe operating at 20-keV accelerating potential, 20-nA beam current measured on brass, and 10-$\mu$m beam diameter, with 40–150-s count times. Additional analyses were done at Stanford University (JEOL 733, 15 keV, 20 nA on Faraday cup) and the Smithsonian Astrophysical Observatory (JEOL 733, 15 keV, 20 nA on Faraday cup). All analyses used natural and synthetic mineral standards with the correction procedure of Bence & Albee (1968), modified by Albee & Ray (1970). Most analyses reported in Table 3 are averages of 3–15 point analyses. Analytical errors are about $\pm 0.20$ oxide wt.% for major elements and $\pm 0.05$–$0.10$ oxide wt.% for minor elements. Apart from the zoning described previously and systematic compositional variations resulting from reactions between intruded magma and wallrocks (Wilshire *et al.*, 1988), minerals are homogeneous within analytical precision.

### Cr-diopside group

Figure 10 and Tables 3–5 show that compositions of olivine and pyroxenes in unreacted peridotite xenoliths of the Cr-diopside group form a tight cluster with $100 \, Mg/(Mg + Fe^{2+})$ values in the range 88–92. In the pyroxenes of the websterites this ratio ranges from 80 to 91
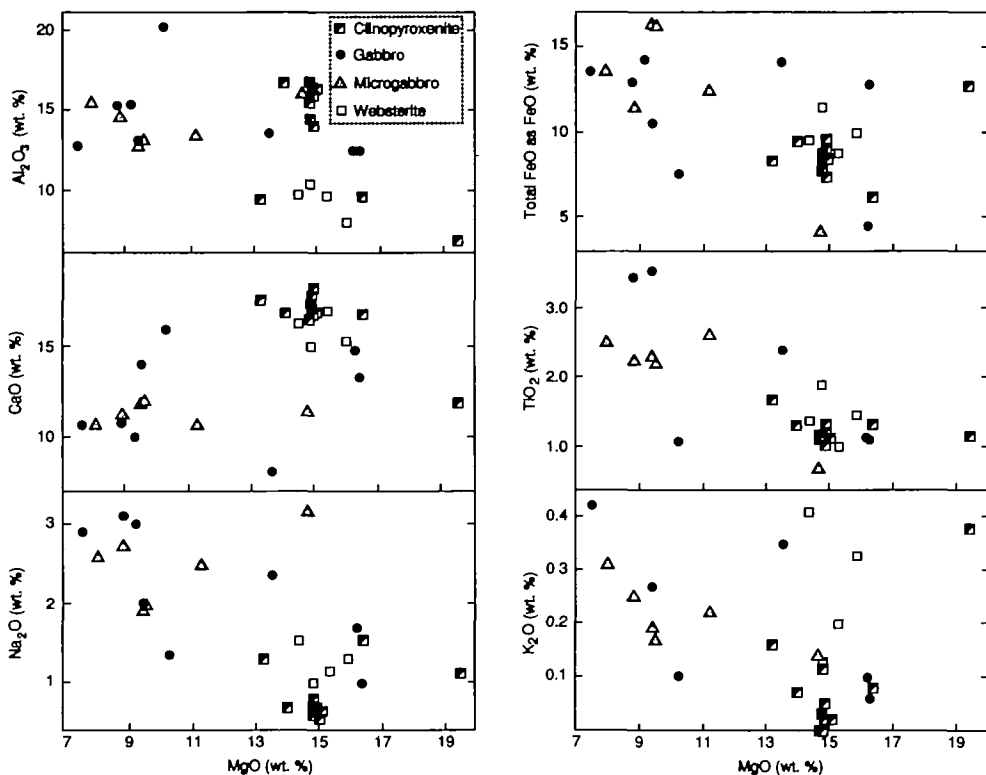
FIG. 9. Variation of major elements in rocks of the Al-augite group with respect to MgO.

(Fig. 10). Spinels (Table 7), although homogeneous within unreacted xenoliths, show a broad range of compositions among different peridotite xenoliths similar to the range reported by McGuire (1988) for Saudi Arabian xenoliths.

McGuire (1988) interpreted a strong positive correlation between modal clinopyroxene + spinel with alumina content of clinopyroxene as an effect of different degrees of partial melt extraction; the expected increase of Cr in spinel (Mysen & Boettcher, 1975) during such a process is less systematic. In Fig. 11, the alumina content of clinopyroxene in Cr-diopside peridotites from Cima is plotted against modal clinopyroxene + spinel and compared with McGuire's (1988) data. The two rock groups show a similar trend, and the Cr/(Cr + Al) ratios of Cima spinels are consistent with the interpretation that the compositional variations reflect degree of partial melt extraction. Cr-diopside websterites in both the Cima and Saudi Arabian occurrences are interpreted as crystallization products of the extracted melts.

The less magnesian compositions of Cr-diopside websterites may be the result in part of reaction with infiltrated melt, but the most magnesian sample analyzed contains introduced plagioclase. Plagioclase in infiltrated Cr-diopside peridotites ranges from $An_{48}$ to $An_{66}$ (Fig. 10; Table 6) with Or contents of 0–1%. Amphibole in one websterite is titanian pargasite.

### Green-pyroxene group

Pyroxenes of this group have $100 \, Mg/(Mg + Fe^{2+})$ ranging from 70 to 82 (Fig. 10; Table 5), with a tendency toward more Fe-rich compositions through the sequence from
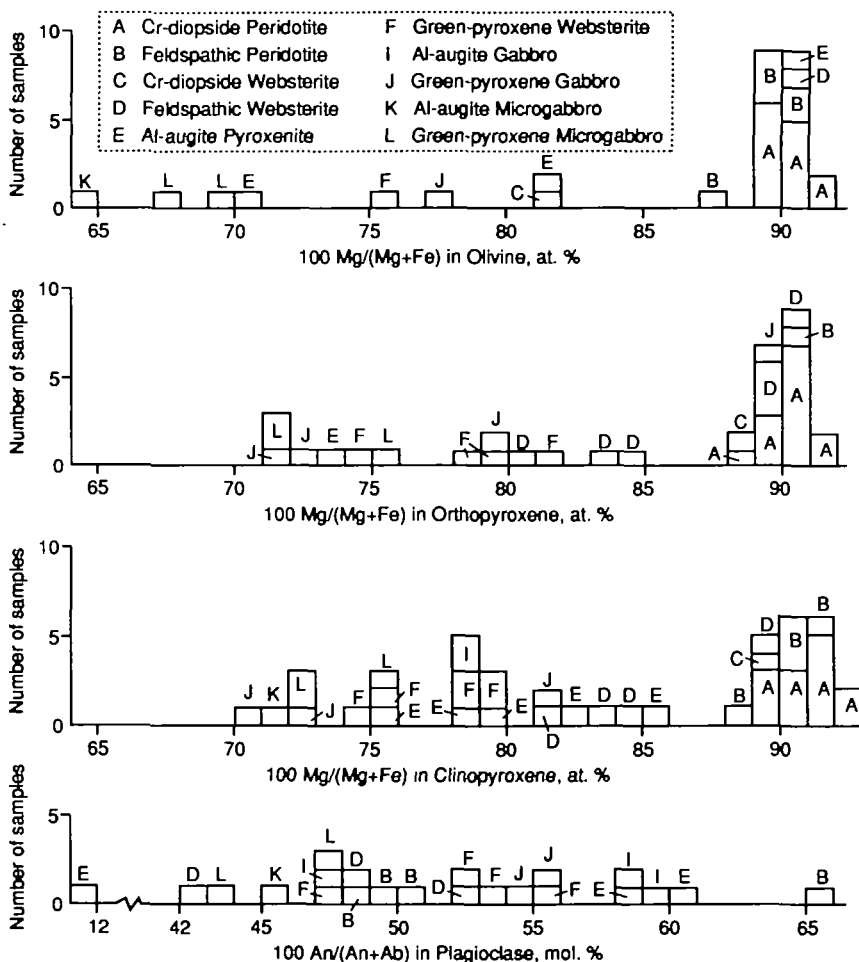
FIG. 10. Histograms showing lithologic distributions of 100 Mg/(Mg + Fe$^{2+}$) for olivine, clinopyroxene, ortho-pyroxene, and An content of plagioclase.
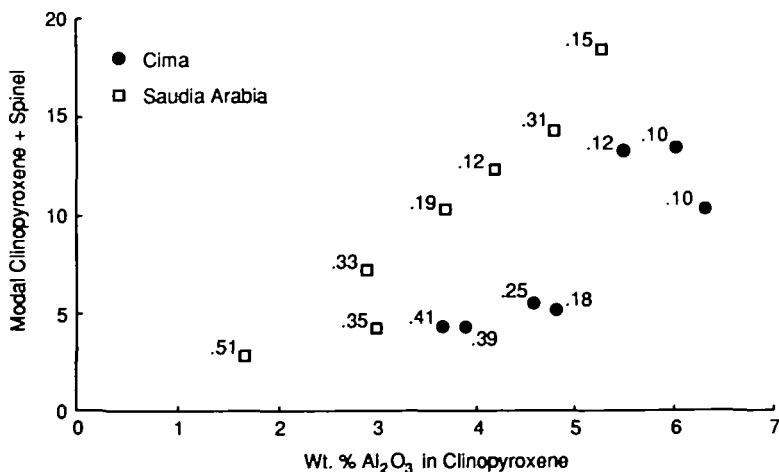


FIG. 11. Modal clinopyroxene + spinel in Cr-diopside peridotites plotted against Al$_2$O$_3$ (wt.%) in clinopyroxene. Numbers indicate Cr/(Cr + Al) in spinel. Data from McGuire (1988) are shown for comparison.

TABLE 3

*Mineral composition data for Cima xenoliths*

| Rock type | Clinopyroxene and orthopyroxene | | | | | | Plagioclase | | | Olivine |
|---|---|---|---|---|---|---|---|---|---|---|
|  | CaO | MgO | FeO | $TiO_2$ | $Al_2O_3$ | $Cr_2O_3$ | An | Ab | Or | Fo |
| | | | *Cr-diopside group* | | | | | | | |
| Lherzolite | | | | | | | | | | |
| Cpx | 45–47 | 48–51 | 4–5 | 0·23–0·62 | 3·7–6·3 | 0·54–1·6 | | | | |
| Opx | 1–2 | 88–90 | 8–11 | 0·06–0·13 | 2·3–4·3 | 0·30–0·52 | | | | |
| Ol | | | | | | | | | | 89–91 |
| Websterite | | | | | | | | | | |
| Cpx | 44–46 | 47–49 | 5–9 | 0·49–0·85 | 4·0–6·5 | 0·17–0·75 | | | | |
| Opx | 2 | 82–89 | 9–16 | 0·13–0·23 | 2·6–3·8 | 0·05–0·38 | | | | |
| | | | *Feldspathic Cr-diopside lherzolite* | | | | | | | |
| Cpx | 44–47 | 48–49 | 5–7 | 0·17–0·92 | 5·0–5·9 | 0·56–0·76 | | | | |
| Opx | 1–2 | 88–90 | 9–10 | 0·10–0·21 | 3·8–4·0 | 0·22–0·37 | | | | |
| Pc | | | | | | | 49–66 | 33–50 | 0–1 | |
| Ol | | | | | | | | | | 88–90 |
| | | | *Green-pyroxene group* | | | | | | | |
| Websterite | | | | | | | | | | |
| Cpx | 39–44 | 42–48 | 12–14 | 0·90–1·4 | 4·7–6·2 | 0·17–0·37 | | | | |
| Opx | 2–3 | 72–80 | 17–25 | 0·25–0·33 | 2·7–3·5 | 0·18–0·36 | | | | |
| Pc | | | | | | | 48–56 | 42–50 | 1–2 | |
| Gabbro | | | | | | | | | | |
| Cpx | 41–44 | 40–46 | 10–26 | 0·52–1·3 | 2·6–6·4 | 0·06–0·38 | | | | |
| Opx | 2–5 | 69–88 | 10–28 | 0·11–0·46 | 2·4–4·3 | 0·02–0·27 | | | | |
| Pc | | | | | | | 45–56 | 43–53 | 1–2 | |
| Ol | | | | | | | | | | 77 |
| Micro-gabbro | | | | | | | | | | |
| Cpx | 40–42 | 43–44 | 14–17 | 1·2–1·3 | 5·4–6·3 | 0·02–0·13 | | | | |
| Opx | 2–3 | 69–74 | 24–28 | 0·28–0·41 | 2·9–4·0 | 0·01–0·11 | | | | |
| Pc | | | | | | | 44–48 | 51–56 | 1–2 | |
| Ol | | | | | | | | | | 67–70 |
| | | | *Al-augite group* | | | | | | | |
| Pyroxenite | | | | | | | | | | |
| Cpx | 44–46 | 42–46 | 8–14 | 0·44–1·5 | 4·9–8·4 | 0·01–0·40 | | | | |
| Opx | 2 | 72 | 26 | 0·31 | 4·2 | 0·18 | | | | |
| Pc | | | | | | | 12–61 | 37–66 | 1–22 | |
| Ol | | | | | | | | | | 70–82 |
| Gabbro | | | | | | | | | | |
| Cpx | 45 | 43 | 12 | 1·4–1·6 | 8·5–8·7 | 0 | | | | |
| Opx | — | — | — | — | — | — | | | | |
| Pc | | | | | | | 48–60 | 38–50 | 2 | |
| Micro-gabbro | | | | | | | | | | |
| Cpx | 40 | 43 | 17 | 1·6 | 5·6 | 0·05 | | | | |
| Pc | | | | | | | 45 | 53 | 2 | |
| Ol | | | | | | | | | | 65 |

pyroxenite to gabbro to microgabbro. Limited data on olivine (Fig. 10, Table 4) indicate more Fe-rich compositions ($Fo_{67-70}$) in microgabbro than in pyroxenites and gabbros ($Fo_{75-78}$). Plagioclase ranges from $An_{43}$ to $An_{56}$ with Or contents of 1–2% (Table 6). Plagioclase of microgabbros is at the sodic end of the An range, but there is no distinction between pyroxenite and gabbro. Amphiboles in gabbros of this group are titanian pargasite ($TiO_2$ 2·2–3·8 wt.%), and the oxides are ilmenite and titanomagnetite–ulvöspinel (Tables 3

and 7). One kaersutite megacryst from Cima described by Colville & Novak (in press) has green-pyroxene group clinopyroxene inclusions.

Websterites of the green-pyroxene group bear close textural resemblance to those from Hualalai described by Bohrson & Clague (1988), who interpreted the symplectic texture in clinopyroxene as exsolution. The orthopyroxene lamellae in the Cima samples have the same composition as the large, isolated orthopyroxene euhedra exclusive of the clinopyroxene lamellae in the latter, but the clinopyroxene rims are a little richer in Fe and Ti and poorer in Cr and Ni than the host clinopyroxene of the symplectites, and differ substantially from the bulk composition of symplectite in most components. Bohrson & Clague (1988) interpreted the rims on symplectite grains in the Hualalai xenoliths as having exsolved orthopyroxene, but the textural relations we observe in the Cima xenoliths suggest that the rims might be overgrowths on clusters of anhedral grains of symplectite. The common occurrence of exsolution-free rims on single clinopyroxene and orthopyroxene grains in the absence of symplectic texture may be because of exsolution during cooling (Bohrson & Clague, 1988).

### Al-augite group

Olivine in rocks of this group ranges from $Fo_{65}$ to $Fo_{91}$ (Fig. 10, Table 4). It is uncertain whether the $Fo_{91}$ composition (olivine in a mica–olivine clinopyroxenite) is primary or crystallized from a partial melt in the rock. Clinopyroxene (Fig. 10, Tables 3 and 5) covers the range of 100 $Mg/(Mg + Fe^{2+})$ values of the green-pyroxene group (71–82) and extends to slightly higher values (86). Plagioclase compositions (Table 6) overlap those of the green-pyroxene group ($An_{43-56}$) at both ends, and range from $An_{12}$ to $An_{61}$. The $An_{12}$ feldspar contains 22% Or and is the most potassic composition measured; otherwise, Or contents are 1–2%, like those of the green-pyroxene group. Amphiboles are titanian pargasite and mica is titanian phlogopite. Kaersutite megacrysts that contain clinopyroxene inclusions with compositions like those of Al-augite pyroxenites have been described by Colville & Novak (in press). Oxides are mostly pleonaste (Tables 3 and 7).

### COMPOSITE XENOLITHS

Composite xenoliths from the Cima volcanic field are abundant; more than 250 samples have been collected, and many others were observed but not collected. The composite xenoliths consist of two or more rock types of the same or different groups (Table 8), and in many, there is clear structural evidence (see Wilshire et al., 1988) that one rock type is the host rock for igneous intrusions represented by the other rock types. Table 8 does not cover hundreds more xenoliths in which Cr-diopside peridotite or websterite were infiltrated by magmas without a clear structural (fracture) control on melt distribution. As described in a following section, infiltrated xenoliths are composite in the sense that they consist of irregular concentrations of the introduced phases (plagioclase ± pyroxene; hornblende ± plagioclase ± pyroxene; hornblende ± mica) in contact with normal spinel lherzolite or websterite. Table 8 also lists recrystallized hornblende peridotites in which the distribution of amphibole suggests that an original vein structure was not completely eradicated by the deformation accompanying recrystallization.

Of the samples listed in Table 8, Cr-diopside peridotite is the host for intrusions in 79% (201 samples) and Cr-diopside websterite is the host in another 7% (17 samples). In the remaining 14% (38 samples), various members of the green-pyroxene and Al-augite groups form the host rocks (Table 8). Thirty of the samples with Cr-diopside peridotite as host

## TABLE 4

*Representative microprobe analyses\* (wt.%) of olivine in Cima xenoliths*

| | Cr-diopside group | | | | Green-pyroxene group | | | Al-augite group | |
| | Peridotite | | Websterite | | Websterite | Troctolite | Microgabbro | Wehrlite | Microgabbro |
| Sample | Ki-5-1 | Ki-5-16 | Ki-5-19 | Ki-5-1 | Ci-1-165 | Ci-6-2 | Ki-5-91 | Ci-2-1 | Ki-5-241 |
|---|---|---|---|---|---|---|---|---|---|
| $SiO_2$ | 39·8 | 40·9 | 40·4 | 39·9 | 38·8 | 38·0 | 36·4 | 37·0 | 35·7 |
| FeO | 10·0 | 8·3 | 10·9 | 9·9 | 22·8 | 20·9 | 29·5 | 27·3 | 31·1 |
| MgO | 49·0 | 49·9 | 48·0 | 49·0 | 39·3 | 40·0 | 33·7 | 35·8 | 32·3 |
| CaO | 0·10 | 0·07 | 0·08 | 0·12 | 0·10 | 0·07 | 0·18 | 0·10 | 0·11 |
| MnO | 0·15 | — | — | 0·14 | 0·30 | — | — | — | — |
| NiO | 0·28 | 0·37 | 0·34 | 0·29 | 0·25 | 0·25 | 0·08 | 0·18 | 0·06 |
| Total | 99·33 | 99·54 | 99·72 | 99·35 | 101·55 | 99·22 | 99·86 | 100·38 | 99·27 |
| Fo | 90 | 91 | 89 | 90 | 75 | 77 | 67 | 70 | 65 |

\* Analyses represent averages of 6–10 points per grain for all mineral species.

## TABLE 5

*Representative microprobe analyses (wt.%) of pyroxene in Cima xenoliths*

| | Cr-diopside group peridotite | | | | | | Cr-diopside group websterite | | | |
| Sample | Ki-5-1 | | Ki-5-16 | | Ki-5-10 | | Ki-5-1 | | Ki-5-120 | |
| Phase | opx | cpx | opx | cpx | opx | cpx | opx | cpx | opx | cpx |
|---|---|---|---|---|---|---|---|---|---|---|
| $SiO_2$ | 55·5 | 52·6 | 56·6 | 53·2 | 55·7 | 52·1 | 55·2 | 52·4 | 54·9 | 51·6 |
| $Al_2O_3$ | 3·4 | 4·8 | 2·5 | 3·8 | 4·0 | 6·0 | 3·5 | 4·8 | 2·6 | 4·0 |
| FeO | 6·0 | 2·8 | 5·5 | 2·5 | 7·0 | 3·2 | 6·0 | 2·9 | 10·1 | 5·0 |
| MgO | 34·4 | 16·4 | 34·3 | 16·5 | 32·6 | 15·8 | 34·4 | 16·3 | 30·5 | 15·7 |
| CaO | 0·87 | 21·1 | 0·78 | 20·6 | 0·80 | 21·4 | 0·87 | 21·1 | 0·87 | 21·2 |
| $NaO_2$ | 0·06 | 0·90 | 0·07 | 1·05 | 0·07 | 1·02 | 0·06 | 0·91 | 0·04 | 0·72 |
| $TiO_2$ | 0·08 | 0·37 | 0·09 | 0·32 | 0·13 | 0·59 | 0·07 | 0·34 | 0·13 | 0·49 |
| MnO | — | — | 0·12 | 0·09 | 0·17 | 0·11 | — | — | 0·26 | 0·12 |
| $Cr_2O_3$ | 0·44 | 0·86 | 0·52 | 1·19 | 0·28 | 0·59 | 0·41 | 0·83 | 0·16 | 0·39 |
| NiO | — | — | — | — | — | — | 0·08 | — | 0·09 | 0·07 |
| Total | 100·75 | 99·83 | 100·48 | 99·25 | 100·75 | 100·81 | 100·59 | ¶99·58 | 99·65 | 99·29 |
| CaO | 2 | 46 | 2 | 45 | 1 | 47 | 2 | 46 | 2 | 45 |
| MgO | 89 | 49 | 90 | 51 | 88 | 48 | 89 | 49 | 83 | 47 |
| FeO | 9 | 5 | 8 | 4 | 11 | 5 | 9 | 5 | 15 | 8 |

TABLE 5 (*Continued*)

| Sample | Green-pyroxene group websterite | | | | | | Al-augite group pyroxenite | | |
| | Ci-1-23 | | Ci-1-64 | | Ci-1-165 | | Ci-2-1 | | Ci-9-80 |
| Phase | opx | cpx | opx | cpx | opx | cpx | opx | cpx | cpx |
|---|---|---|---|---|---|---|---|---|---|
| $SiO_2$ | 53·7 | 49·8 | 53·9 | 50·4 | 53·5 | 51·2 | 52·6 | 49·1 | 48·9 |
| $Al_2O_3$ | 2·7 | 5·5 | 3·0 | 5·6 | 3·5 | 4·7 | 4·2 | 6·5 | 8·3 |
| FeO | 11·4 | 6·8 | 12·7 | 7·4 | 13·8 | 7·2 | 16·5 | 8·0 | 6·8 |
| MgO | 29·2 | 15·3 | 28·0 | 16·0 | 27·5 | 15·3 | 26·2 | 13·7 | 14·0 |
| CaO | 1·62 | 19·4 | 1·59 | 17·8 | 1·22 | 19·4 | 1·10 | 19·8 | 20·1 |
| $NaO_2$ | 0·14 | 0·98 | 0·10 | 0·88 | 0·05 | 0·69 | — | 0·76 | 0·81 |
| $TiO_2$ | 0·27 | 1·09 | 0·30 | 1·08 | 0·25 | 0·90 | 0·31 | 1·10 | 1·52 |
| MnO | 0·21 | 0·15 | 0·22 | 0·15 | 0·31 | 0·20 | 0·26 | 0·16 | 0·18 |
| $Cr_2O_3$ | 0·36 | 0·35 | 0·31 | 0·37 | 0·18 | 0·21 | 0·18 | 0·40 | 0·01 |
| NiO | — | — | — | — | 0·10 | 0·06 | — | — | — |
| Total | 99·60 | 99·37 | 100·12 | 99·68 | 101·41 | 99·86 | 101·35 | 99·52 | 100·62 |
| CaO | 3 | 42 | 3 | 39 | 2 | 42 | 2 | 44 | 45 |
| MgO | 80 | 46 | 77 | 48 | 76 | 46 | 72 | 42 | 43 |
| FeO | 17 | 12 | 20 | 13 | 22 | 12 | 26 | 14 | 12 |

TABLE 5 (*Continued*)

| Sample | Green-pyroxene group gabbro | | | | Al-augite group gabbro | | Green-pyroxene group microgabbro | | | | Al-augite group microgabbro |
| | Ki-5-47 | | Ci-1-2 | | Ki-2-28 | Ki-2-113 | Ci-1-2 | | Ki-5-91 | | Ki-5-241 |
| Phase | opx | cpx | opx | cpx | cpx | cpx | opx | cpx | opx | cpx | cpx |
|---|---|---|---|---|---|---|---|---|---|---|---|
| $SiO_2$ | 53·4 | 51·8 | 50·9 | 48·5 | 48·6 | 48·1 | 52·0 | 49·1 | 52·0 | 49·2 | 49·8 |
| $Al_2O_3$ | 2·4 | 2·6 | 4·3 | 6·4 | 8·7 | 8·5 | 4·0 | 6·3 | 3·0 | 5·6 | 5·6 |
| FeO | 16·6 | 10·3 | 17·9 | 9·2 | 6·7 | 6·8 | 15·4 | 8·0 | 18·0 | 9·8 | 10·0 |
| MgO | 25·1 | 13·9 | 24·8 | 13·9 | 13·8 | 13·9 | 26·9 | 14·2 | 24·8 | 14·2 | 14·2 |
| CaO | 2·29 | 20·4 | 1·27 | 18·2 | 20·2 | 20·3 | 1·25 | 18·8 | 1·23 | 18·4 | 18·2 |
| $Na_2O$ | 0·06 | 0·53 | 0·08 | 1·03 | 0·91 | 0·83 | 0·08 | 1·01 | 0·02 | 0·65 | 0·77 |
| $TiO_2$ | 0·32 | 0·52 | 0·46 | 1·29 | 1·38 | 1·62 | 0·38 | 1·24 | 0·28 | 1·15 | 1·55 |
| MnO | 0·29 | 0·24 | 0·33 | 0·20 | 0·16 | 0·17 | 0·27 | 0·16 | 0·36 | 0·24 | 0·26 |
| $Cr_2O_3$ | 0·17 | 0·06 | 0·02 | — | 0·0 | 0·0 | 0·09 | 0·13 | 0·11 | 0·04 | 0·05 |
| NiO | — | — | — | — | — | — | — | — | — | — | — |
| Total | 100·63 | 100·35 | 100·06 | 98·81 | 100·45 | 100·22 | 100·37 | 98·94 | 98·80 | 99·28 | 100·43 |
| CaO | 5 | 43 | 3 | 41 | 45 | 45 | 2 | 42 | 3 | 40 | 40 |
| MgO | 70 | 40 | 69 | 43 | 43 | 43 | 74 | 44 | 69 | 43 | 43 |
| FeO | 25 | 17 | 28 | 26 | 12 | 12 | 24 | 14 | 28 | 17 | 17 |

TABLE 6

*Representative microprobe analyses (wt.%) of feldspar in Cima xenoliths*

| Sample | Cr-diopside group Peridotite Ki-5-39 | Websterite Ki-5-4 | Websterite Ci-1-64 | Ci-1-165 | Green-pyroxene group Gabbro Ki-5-47 | Troctolite Ci-6-2 | Microgabbro Ki-5-91 | Al-augite group Gabbro Ki-2-28 | Microgabbro Ki-5-241 |
|---|---|---|---|---|---|---|---|---|---|
| $SiO_2$ | 55·3 | 54·6 | 54·5 | 54·9 | 54·0 | 53·9 | 54·9 | 52·8 | 56·6 |
| $Al_2O_3$ | 27·5 | 28·5 | 28·7 | 28·4 | 28·7 | 29·6 | 27·4 | 30·1 | 27·1 |
| FeO | 0·11 | 0·26 | 0·22 | 0·18 | 0·23 | 0·16 | 0·26 | 0·21 | 0·23 |
| CaO | 10·0 | 11·0 | 10·9 | 11·0 | 11·4 | 11·6 | 9·9 | 12·4 | 9·3 |
| $Na_2O$ | 5·3 | 5·1 | 5·3 | 4·6 | 5·1 | 4·9 | 5·8 | 4·5 | 6·1 |
| $K_2O$ | 0·12 | 0·38 | 0·22 | 0·27 | 0·27 | 0·26 | 0·16 | 0·32 | 0·36 |
| Total | 98·33 | 99·84 | 99·84 | 99·35 | 99·70 | 100·42 | 98·42 | 100·33 | 99·69 |
| An | 51 | 53 | 53 | 56 | 55 | 56 | 48 | 59 | 45 |
| Ab | 49 | 45 | 46 | 42 | 44 | 43 | | 39 | 53 |
| Or | 0 | 2 | 1 | 2 | 1 | 1 | | 2 | 2 |

TABLE 7

*Representative microprobe analyses (wt.%) of oxides in Cima xenoliths*

| Sample | Cr-diopside group Peridotite Ki-5-16 | Ki-5-19 | Websterite Ci-1-23 | Ci-1-165 | Green-pyroxene group Gabbro Ki-5-47 | Troctolite Ci-6-2 | Microgabbro Ki-5-98 | Al-augite group Pyroxenite Ci-9-80 | Gabbro Ki-2-28 |
|---|---|---|---|---|---|---|---|---|---|
| $SiO_2$ | — | 0·01 | — | 0·03 | — | 0·03 | 0·09 | — | 0·0 |
| $Al_2O_3$ | 34·8 | 57·2 | 0·76 | 0·48 | 0·60 | 0·41 | 5·7 | 60·8 | 61·3 |
| FeO | 13·8 | 11·8 | 39·7 | 36·3 | 38·3 | 34·6 | 65·1 | 21·2 | 21·1 |
| MgO | 17·5 | 20·5 | 7·7 | 8·5 | 8·1 | 9·8 | 6·0 | 17·7 | 17·5 |
| CaO | 0·0 | 0·0 | 0·03 | 0·05 | 0·04 | 0·06 | 0·07 | 0·0 | 0·0 |
| $TiO_2$ | 0·24 | 0·15 | 49·0 | 54·6 | 51·5 | 53·5 | 18·3 | 0·47 | 0·38 |
| MnO | 0·20 | 0·12 | 0·26 | 0·46 | 0·27 | 0·32 | 0·37 | 0·15 | 0·14 |
| $Cr_2O_3$ | 33·2 | 9·4 | 0·75 | 0·24 | 0·25 | 0·41 | 0·88 | 0·04 | 0·02 |
| Total | 99·74 | 99·27 | 98·20 | 100·66 | 99·06 | 99·13 | 96·51 | 100·36 | 100·44 |
| *mg*-no. | 69 | 76 | 26 | 30 | 28 | 34 | 14 | 60 | 60 |

## TABLE 8

*Rock types in composite Cima xenoliths*

| Group | Lithology | No. of samples |
|---|---|---|
| | *Composite with Cr-diopside peridotite** | |
| Cr-diopside | Websterite, olivine websterite | 28 |
| | Orthopyroxenite | 2 |
| Green-pyroxene | Websterite | 14 |
| | Hornblende websterite | 3 |
| | Gabbro | 2 |
| Al-augite | Clinopyroxenite | 9 |
| | Wehrlite | 1 |
| | Gabbro | 7 |
| | Micrograbbro | 1 |
| Group not | Hornblendite (veins) | 46 |
| identified | Hornblendite (recrystallized) | 31 |
| | Phlogopite (veins) | 10 |
| | Pyroxenite | 7 |
| | Gabbro | 26 |
| | Hornblende biotite gabbro | 1 |
| | Hornblende gabbro | 1 |
| | Microgabbro | 10 |
| | Hornblende microgabbro | 2 |
| | *Composite with Cr-diopside websterite* | |
| Cr-diopside | Olivine orthopyroxenite | 1 |
| Green-pyroxene | Microgabbro | 2 |
| Al-augite | Clinopyroxenite | 2 |
| Group not | Hornblendite (veins) | 6 |
| identified | Hornblendite (recrystallized) | 1 |
| | Gabbro | 3 |
| | Hornblende gabbro | 1 |
| | Microgabbro | 1 |
| | *Composite with green-pyroxene websterite* | |
| Green-pyroxene | Gabbro | 8 |
| | Olivine pyroxenite | 1 |
| | Hornblende gabbro | 1 |
| Al-augite | Gabbro | 2 |
| Group not | Gabbro | 1 |
| identified | Pyroxenite | 1 |
| | *Composite with green-pyroxene gabbro* | |
| Green-pyroxene | Microgabbro | 5 |
| | *Composite with Al-augite pyroxenite* | |
| Al-augite | Gabbro | 8 |
| | Wehrlite | 1 |
| | *Composite with Al-augite wehrlite* | |
| Al-augite | Gabbro | 3 |
| | *Composite with Al-augite gabbro* | |
| Al-augite | Microgabbro | 2 |
| | Hornblende microgabbro | 1 |
| | *Composite with transitional pyroxenite* | |
| Transitional | Microgabbro | 1 |
| | *Composite with unidentified pyroxenite* | |
| Group not identified | Gabbro | 1 |
| | *Composite with unidentified gabbro* | |
| Group not identified | Microgabbro | 2 |

* Rock type identified at head of each grouping is observed or inferred to be the host rock for intrusions of the types identified below the heading.

contain Cr-diopside pyroxenite dikes. Members of either the green-pyroxene or Al-augite groups are intrusive into a green-pyroxene group host, but only members of the Al-augite group have been observed to cut other members of that group. It is evident from Table 8 that all rock types except the most uncommon of the green-pyroxene and Al-augite groups occur as intrusions in Cr-diopside lherzolite. The sequence of intrusion into Cr-diopside peridotite, inferred from crosscutting relations, is Cr-diopside pyroxenite–green-pyroxene group–Al-augite group. Multiple intrusions of magmas representing the green-pyroxene and Al-augite groups do occur, but no evidence has been observed in Cima xenoliths of multiple intrusions of magma representing Cr-diopside websterites as seen elsewhere (Wilshire *et al.*, 1988).

## MAGMATIC INFILTRATION

Perhaps 25% of Cr-diopside lherzolites and pyroxenites at Cima contain diffuse concentrations of plagioclase and/or amphibole in roughly planar concentrations or anastomosing networks. There are gradations in sharpness of contacts between dikes and products of grain-boundary melt infiltration (Fig. 5b). The mode of occurrence of these concentrations is like that of 'indigenous' veins of the Lanzo plagioclase peridotite massif described by Boudier & Nicolas (1977), but the concentrations in Cima xenoliths are much more irregular in distribution, even within single xenoliths. The infiltrating melts either were basaltic, or were felsic or amphibole-rich differentiates of basaltic magma. Plagioclase may or may not be accompanied by some new pyroxene which is indistinguishable in hand specimen but in thin section is distinguishable in some cases by the presence of exsolution lamellae and by its less calcic composition. Plagioclase, pargasite, and phlogopite occur as thin, irregular stringers and as dispersed grains that may or may not be in textural equilibrium with the peridotite. The distribution of these minerals is heterogeneous within a single hand specimen so that one part of a xenolith may be relatively rich in these components and another entirely free of them. The parts of the xenoliths free of plagioclase and hydrous minerals are identical to homogeneous Cr-diopside peridotite and websterite xenoliths, whereas the parts that contain them have modified mineral compositions (more Fe-rich silicates, more aluminous spinels; Wilshire *et al.*, 1988). Disequilibrium between plagioclase and amphibole and the host peridotite is also shown by common coronal relations between these minerals, either in thin stringers or as dispersed grains, and spinel. However, in approximately half of the infiltrated peridotite xenoliths, the peridotite has been penetratively deformed and recrystallized after introduction of plagioclase (Fig. 5c) and amphibole (Fig. 5d). These deformed rocks typically have porphyroclastic–tabular or tabular textures and the plagioclase and amphibole are in textural equilibrium with the peridotite; that is, these minerals have the same sizes, shapes, and preferred orientations as the peridotite minerals, and show no reaction relation with them.

The proportions of the different textural variants of peridotite containing plagioclase and/or hydrous minerals are shown in Table 9. Of 35 samples examined in thin section, 51% are undeformed to weakly deformed (weakly foliated and transitional allotriomorphic-granular/mosaic categories). In hand specimen, deformation and recrystallization are much easier to identify in the amphibole-bearing than the plagioclase-bearing peridotite. Thirty-one of 77 peridotite xenoliths containing dispersed amphibole or hornblendite veins have been deformed and recrystallized; thus, there appears to be no connection between deformation and the presence of plagioclase or hydrous minerals in Cr-diopside peridotite or pyroxenite as has been reported elsewhere (Downes, 1987; Downes & Dupuy, 1987; Nicolas *et al.*, 1987). Moreover, despite the evidence for infiltration of shear zones in some xenoliths, the suggestion by those authors that infiltrating magmas prefer deformed zones is

TABLE 9

*Proportions (percentages) of the different textural variants of peridotite with and without hornblende and plagioclase*

| Texture | No hbl, pc | Hbl ± pc |
|---|---|---|
| Allotriomorphic–granular | 24 | 20 |
| Weakly foliated allotriomorphic–granular | 11 | 3 |
| Transitional allotriomorphic–granular/mosaic | 29 | 28 |
| Porphyroclastic–mosaic | 18 | 23 |
| Porphyroclastic–tabular | 13 | 17 |
| Tabular | 5 | 9 |

38 samples without hbl or pc; 35 samples with hbl and/or pc.

TABLE 10

*Temperature estimate for Cima xenoliths, by the method of Wells (1977)*

| Sample | Rock type | T(°C) | Sample | Rock type | T(°C) |
|---|---|---|---|---|---|
| | Cr-diopside group | | | Reacted peridotite | |
| Ki-5-4 | Lherzolite | 885 | Ki-5-39 | | 965 |
| Ki-5-82 | Lherzolite | 940 | Ki-5-127 | | 995 |
| Ki-5-48 | Lherzolite | 955 | Ki-5-139 | | 1005 |
| Ki-5-52 | Lherzolite | 960 | | Green-pyroxene group | |
| Ki-5-2 | Lherzolite | 960 | Ki-5-229 | Websterite | 970 |
| Ki-5-62 | Lherzolite | 960 | Ci-1-165 | Olivine websterite | 1015 |
| Ki-5-35 | Lherzolite | 965 | Ci-1-359 | Websterite | 1075 |
| Ki-5-19 | Lherzolite | 970 | Ci-1-64 | Websterite | 1095 |
| Ki-5-130 | Lherzolite | 975 | Ki-5-47 | Gabbro | 965 |
| Ki-5-37 | Lherzolite | 980 | Ci-1-2 | Gabbro | 1020 |
| Ki-5-235 | Lherzolite | 995 | Ci-1-23 | Gabbro | 1030 |
| Ki-5-11 | Lherzolite | 1015 | Ci-6-2 | Troctolite | 1015 |
| Ki-5-120 | Websterite | 975 | Ki-5-98 | Microgabbro | 1035 |
| Ci-9-7 | Websterite | 990 | Ki-5-91 | Microgabbro | 1035 |
| Ki-5-1 | Websterite | 995 | Ci-1-11 | Microgabbro | 1045 |
| Ki-5-31 | Feldspathic lherzolite | 960 | | Al-augite group | |
| Ki-5-12 | Feldspathic lherzolite | 970 | Ci-2-1 | Pyroxenite | 980 |
| Ki-5-45 | Feldspathic websterite | 1010 | Ci-1-354 | Pyroxenite | 995 |
| | | | Ci-1-31 | Gabbro | 975 |

not supported by the many Cima examples (~40–50%) in which deformation followed crystallization of the introduced melts.

Several xenoliths show magmatic infiltration of shear zones in Cr-diopside group rocks. Plagioclase is an important constituent in all of these products of infiltration, and all shear zones contain large quantities of granulated peridotite and pyroxenite. In one sample (Ci-1-262), two fragments of Cr-diopside websterite are in contact with pyroxene microgabbro, which in turn is in relatively sharp contact with olivine-rich microgabbro. In thin section, the dominant pyroxenes in the microgabbro adjacent to the Cr-diopside websterite are seen to be angular fragments similar to, but of smaller grain size than, the websterite. As the contact with olivine-rich microgabbro is approached, there is an increasing proportion, in a mixed websterite–peridotite zone, of tabular olivine grains aligned parallel to the contact. Across the contact, the rock has abundant tabular olivine, also oriented parallel to the contact. The

olivines are undeformed. Plagioclase grains are either tabular and in textural equilibrium, or equidimensional and weakly zoned. This xenolith is interpreted as a Cr-diopside websterite dike cutting peridotite that was sheared along the dike contact and infiltrated by magma. Shearing was lubricated by the magma, and crystallization of the melt and recrystallization of peridotite proceeded during deformation. In other infiltrated shear zones in peridotite, olivine derived from the peridotite is not recrystallized and is identified by angular shapes and internal deformation features.

Infiltration of rocks of the green-pyroxene or Al-augite group rocks would be difficult to detect, but may be anticipated in the light of the evidence favoring multiple intrusions in both groups and their temporal relations. Ambiguous evidence of such infiltration is found in a few Al-augite clinopyroxenites in which coarse plagioclase + olivine coronas on spinel are irregularly distributed through the pyroxenite. If the coronas were a reaction response to reduced pressure as is commonly inferred, the irregular distribution in single xenoliths would be difficult to explain. Coronal relations have not been found in the green-pyroxene pyroxenites with their sparse oxides. However, one sample of green-pyroxene olivine websterite that is intruded by Al-augite gabbro dikes appears macroscopically to have been infiltrated along a zone at a high angle to the dike by melts from which plagioclase crystallized. Hydrous infiltration of green-pyroxene pyroxenites and gabbros may be indicated by oriented amphibole inclusions in pyroxenes, and by crystallization of apatite and amphibole in patches of vesicular quenched melt in these rocks.

## INCOMPLETE CRYSTALLIZATION OF IGNEOUS ROCKS AND MELTING PHENOMENA IN METAMORPHIC AND IGNEOUS XENOLITHS

Incomplete crystallization of igneous rocks and partial melting of metamorphic and igneous rocks are common phenomena in Cima xenoliths. Representatives of all principal rock types are affected. Distinction between arrested crystallization and the effects of melting of an igneous rock, based on textural relations, is not simple. Melts that occupy interstitial areas with unembayed adjacent mineral grains are here interpreted as quenched residual melts, but some rocks with substantial melt fractions that satisfy these criteria also have glass-lined vesicles inside primary minerals, and their pyroxenes may have exsolved phases. Melting textures are less ambiguous. Some are analogous to secondary-mineral replacement textures in that quenched melts contain irregularly embayed relics of primary minerals. Selective melting of particular minerals is represented by quench products which have the distribution and form of the melted mineral or by glass sieving of particular mineral species. In other xenoliths, melting has destroyed large areas of the original fabric of the rock.

The least ambiguous cases of arrested crystallization are represented by rocks of the Al-augite group. Interstitial glass in thin (2 mm) veins of Al-augite olivine microgabbro or feldspathic micropyroxenite cutting Cr-diopside lherzolite indicates close temporal relations between such injections and the volcanism.

Melting phenomena are very common and involve the metamorphosed peridotites and pyroxenites of the Cr-diopside group as well as the igneous rocks. Although there is a general order of susceptibility of minerals to melting, the behavior of any mineral in the melting process is sensitive to the total assemblage. For example, amphibole in gabbro or pyroxenite dikes in peridotite is commonly melted, whereas hornblendite derivatives of such intrusions that were emplaced in the peridotite or in Cr-diopside pyroxenite may remain intact in the same xenolith. It would appear that the temperature rose above the hornblende gabbro solidus but remained below the hornblende peridotite solidus. Some composite xenoliths

show relatively extensive melting of hornblende-bearing, feldspathic pyroxenite or gabbro intrusions in harzburgite but show no visible effects in the peridotite.

The order of melting in gabbro and pyroxenite xenoliths is not directly related to the order of crystallization. In both Al-augite and green-pyroxene group xenoliths, the first phases to melt are hydrous minerals and spinels, then orthopyroxene, then clinopyroxene, and plagioclase is last. The reluctance of plagioclase to melt, whether it crystallized early or late, is evident both in intrusive gabbros in peridotite and in isolated gabbro xenoliths.

Quenched melts free of new crystalline products are rare. Most glasses contain various proportions of olivine, plagioclase, opaque oxides, and, less commonly, clinopyroxene. There is a gradation from fine-grained quench crystals to coarse-grained new-formed mineral intergrowths with diminishing proportions of glass. The assemblage olivine–plagioclase is omnipresent in crystallized melts, irrespective of the mineralogy of the parent rock, and, where formed at the expense of Cr-diopside or green-pyroxene websterite, it may represent a lower pressure than the parent assemblage (Wilshire & Kirby, 1989). The occurrence of coarse, nonskeletal products of crystallization of partial melts indicates that the crystallization occurred over a period of time and that the melting predates incorporation of the xenoliths in the host basalts. Decompression melting resulting from entrainment of xenoliths in the host magma (Padovani & Carter, 1977) does not appear to be a primary cause of the melting in such cases.

## TEMPERATURE AND PRESSURE CONDITIONS IN THE XENOLITH SOURCE AREA

A variety of geothermometers apply to the mineral assemblages present in Cima xenoliths, and their comparative merits have been thoroughly discussed (Carswell & Gibb, 1987; Finnerty & Boyd, 1987; McGuire, 1988). Because of its lack of correlation with $Fe^{3+}$, and uncertainty in determining $Fe^{3+}$ (Gutmann, 1986; McGuire, 1988), the Wells (1977) geothermometer is preferred for use with the Cima xenoliths (Table 10). Temperatures calculated from other geothermometers agree closely with Wells' two-pyroxene temperatures. Although the common presence of partial melts in the xenoliths indicates above-solidus temperatures, the exsolved pyroxenes show no signs of having equilibrated to these temperatures. Thus, the temperatures reported all reflect subsolidus conditions before melting.

There are no suitable tested geobarometers that apply to the Cima xenoliths. However, mineral assemblages place approximate limits on depth of origin of some of the rocks. The depths of origin of nonfeldspathic spinel peridotites are bracketed by the spinel peridotite stability field, ~8–16 kb at 900–1100 °C in simple experimental systems (Gasparik, 1984). Addition of $Cr_2O_3$ to simple experimental compositions extends the stability field of spinel peridotite to higher $P$ (O'Neill, 1981; Chatterjee & Terhart, 1985). Based on spinel $Cr_2O_3$ contents alone (9·4–33·8 wt.%), Cima spinel peridotites may have been stable to maximum pressures as high as ~25 kb. Recrystallization of infiltrated peridotites to assemblages with plagioclase in textural equilibrium indicates that those rocks equilibrated in the plagioclase peridotite field, or at ~8–11 kb between 800 and 1200 °C (Green & Ringwood, 1967a; Jaques & Green, 1980).

According to limited experimental data on mafic xenoliths (Irving, 1974), feldspathic spinel websterites of the green-pyroxene group would be stable between ~8 and 14 kb at temperatures of 900–1200 °C. Above these pressures, garnet-bearing assemblages, which do not occur at Cima, would be stable, and below these pressures, olivine–plagioclase assemblages would be stable. Olivine gabbros do occur, and some form intrusions in

peridotite. These *T, P* comparisons can only be regarded as approximate, however, because there are substantial differences in bulk composition between Cima xenoliths and those studied by Irving (1974), and because the Cima xenoliths did not achieve subsolidus equilibrium.

These lines of information indicate that part of the Cima xenolith assemblage formed at pressures near that of the present local seismic Moho at ~27–30 km (Gibbs & Roller, 1966; Hauser *et al.*, 1987). This interpretation is supported by the presence of recrystallized feldspathic peridotites whose stability field straddles the present Moho, and by the presence of gabbroic intrusions in peridotite, which could not persist far below the Moho. It is possible, however, that unmodified spinel peridotites and olivine gabbros came from much deeper (to ~75 km) and somewhat shallower depths, respectively.

## DISCUSSION

Of the two groups of igneous xenoliths, members of the green-pyroxene group are dominant at Cima. Evidence from crosscutting relations indicates that the green-pyroxene group is older than the Al-augite group. The existence of composite xenoliths containing members of both groups, as well as the common occurrence of composite xenoliths of spinel and plagioclase peridotite and members of either the green-pyroxene or Al-augite group, further suggests that igneous rocks of both groups can occupy the same or similar depth intervals in the lithosphere.

The igneous rocks occur in the upper mantle as dike complexes, infiltrated shear zones, and diffuse, grain-boundary infiltration zones, for all of which there is abundant direct evidence. Neither the seismic data nor the structural relations in composite xenoliths support the existence of large sills in the upper mantle, such as has been postulated by Griffin & O'Reilly (1987) for other areas (Wilshire, 1990). It is not necessary to postulate thick differentiated intrusions to yield the variety of related rock types in each group because the main rock types occur in dikes as thin as a few centimeters. In addition, the surprising abundance of composite igneous xenoliths in which one lithology forms irregular intrusions in another of the same group suggests either many relatively small intrusions or a very dynamic system during crystallization. The micrograbbros could represent chilled border facies of intrusions, as have been observed in some ophiolite complexes (Pederson, 1986) and inferred for some stratiform intrusions (Himmelberg & Ford, 1983). They could also occur as irregularly distributed pockets in coarse-grained gabbro dikes such as occur in the Lanzo (Bodinier *et al.*, 1986) and Monte Maggiore (Jackson & Ohnenstetter, 1981) peridotite massifs. In either case, the relatively common occurrence of microgabbros at Cima also suggests the occurrence of abundant small intrusions rather than a few thick intrusions.

Although rocks of the green-pyroxene and Al-augite groups show substantial overlap of compositional trends, rocks of the green-pyroxene group typically are hypersthene-normative, and some gabbros are quartz-normative, whereas rocks of the Al-augite group commonly are ne-normative (Table 2). The abundance of orthopyroxene and its common occurrence as a liquidus or near-liquidus phase in green-pyroxene rocks indicates tholeiitic or calcalkalic parentage, whereas the generally low abundance or absence of orthopyroxene in Al-augite rocks indicates alkali basaltic parentage. In addition, the well-developed exsolution textures in pyroxenes of the green-pyroxene group are hallmarks of tholeiitic plutonic rocks, and their essential absence in pyroxenes of the Al-augite group is a hallmark of alkali basaltic intrusions.

Comparison of inferred crystallization sequences in the xenoliths with experimentally determined sequences in tholeiitic and alkaline basalt melts also assists in identification of

the parental magmas. The phase diagrams of Green & Ringwood (1967*b*) for natural tholeiitic and alkaline basalt show that orthopyroxene is a liquidus phase in tholeiitic basalt at ~13 kb, and crystallizes with plagioclase below the liquidus between 9 and 12 kb, whereas in alkaline basalt, orthopyroxene forms in only small amounts at ~13 kb but does not coexist with plagioclase at any pressure up to 27 kb. These relations support our inference that rocks of the green-pyroxene group are derived from tholeiitic (or calcalkalic) parent magmas and that most rocks of the Al-augite group are products of alkalic parent magmas. However, in simple experimental systems (Windom & Boettcher, 1981), there is a broad orthopyroxene field on the liquidus of alkalic melts at 28 kb with an approximate lower pressure limit of 11 kb (in the system $CaO–MgO–Al_2O_3–SiO_2–Na_2O$; Presnall & Hoover, 1987) to 12 kb (Presnall *et al.*, 1978). In addition, the two-pyroxene subgroup of the Al-augite group indicates that alkaline basalt compositions exist from which abundant orthopyroxene can crystallize at pressures below the stability of garnet in pyroxenite.

On the basis of the apparent relative ages of green-pyroxene and Al-augite intrusions, we conclude that the magmatism beneath Cima represented by the xenoliths began with emplacement of relatively voluminous tholeiitic or calcalkalic magmas and changed to yield less voluminous alkali basaltic magmas. This transition corresponds both in relative age and in magma volumes to stages 2 and 4 in the eruptive cycles of Hawaiian volcanoes (Clague & Dalrymple, 1987). The sequence, but not relative volumes, also corresponds to eruptives related to Red Sea rifting (Coleman *et al.*, 1983; Coleman, 1984). However, a sequence from tholeiitic to alkalic eruption has many exceptions (see, for example, Presnall *et al.*, 1978). Minor Cima volcanic rocks of possible tholeiitic parentage have been dated at 12·8 Ma, and similar rocks are more widespread to the north and west in the Shadow Valley sequence (Reynolds & Nance, 1988).

In view of the absence of metamorphic overprinting on rocks of the green-pyroxene and Al-augite groups, it seems unlikely that they formed under radically different conditions of crustal thickness that existed before Tertiary extension. This conclusion is further supported by the mineral assemblages in the dikes in upper-mantle peridotite that are appropriate to the present position of the upper mantle inferred from geophysical data. Although the ages of upper-mantle magmatism represented by the green-pyroxene and Al-augite group dikes are not known, the igneous textures and mineral assemblages of the dikes in peridotite indicate that both groups represent Tertiary igneous activity, presumably in response to mid-Tertiary extension.

The extent of magmatic additions to the lower crust beneath Cima are not constrained because the pertinent rock types, olivine gabbro and troctolite, are both stable at all depths from the Moho to the surface. Because there are no granulite xenoliths present at Cima, major underplating of the crust by multiple intrusions would require a continuous build-up of igneous additions with little or no interleaved pre-existing crustal rock. A lower crustal section ~13 km thick consisting of rocks with $V_p$ of 6·8 km/s is inferred from a nearby refraction profile (Gibbs & Roller, 1966). The xenoliths of igneous rocks at Cima, despite their generally mafic compositions, could have $V_p$ values of this order, particularly because the extensive partial melting, sieving of the rocks by cavities from microscopic to 2·5 cm in size, and the close-spaced tensile fractures should all result in velocities lower than would be calculated on the basis of mineralogy (Wilshire & Kirby, 1989; Wilshire, 1990); fractures and cavities would necessarily be filled with fluids at the inferred depths of origin. Magnetotelluric and seismic studies elsewhere also suggest the importance of fluids in lower crustal rocks in modifying bulk rock velocities (Hyndman & Klemperer, 1989; Hyndman & Shearer, 1989). One alternative is that the Cima xenolith assemblage represents only a limited crustal section and is not representative; another is that the majority of Cima xenoliths were derived

from beneath the seismic Moho, a conclusion reached by Gutmann (1986) for feldspathic ultramafic xenoliths in the Pinacate volcanic field. It is clear from the Cima composite gabbro/peridotite samples that some rocks typical of the Cima crustal assemblage are derived from below the Moho. This space, however, is also occupied by feldspathic peridotite which must be restricted to a zone immediately below the present Moho. Boettcher (1986) concluded, on the basis of isotopic dissimilarity between the host basalts and one xenolith of two-pyroxene gabbro and from the absence of schists, gneisses, and amphibolites in the xenolith assemblage, that igneous rocks like the xenoliths constitute most of the crust beneath Cima. In our view, however, the high densities of the mafic xenoliths preclude their representing mid- and upper-crustal rocks.

A magmatically enriched transition zone below the Moho as much as 15 km thick appears permissible on the basis of mineral assemblages in the pyroxenite dikes in spinel peridotite, the limiting factor being the garnet-in reaction in websterite compositions (O'Reilly & Griffin, 1985; McGuire, 1988). If magmatic additions have the complex dike forms observed in Cima composite samples, the mantle would be nonreflective, as in fact it is in reflection profiles straddling the Cima field (Klemperer *et al.*, 1986; Hauser *et al.*, 1987). Textural equilibrium among all mineral phases in deformed and recrystallized peridotite that had been infiltrated by melts from which plagioclase crystallized indicates stability of plagioclase peridotite below the Moho at Cima, through about a 5-km thickness of the uppermost mantle.

## CONCLUSIONS

Abundant composite xenoliths indicate that the uppermost mantle beneath the Cima volcanic field is composed of a complex network of intersecting dikes in spinel- and plagioclase-facies peridotite. The dikes, and associated products of intergranular infiltration of peridotite, represent at least three periods of magmatism. Representatives of the two youngest periods of magmatism retain igneous textures and may have been emplaced during Cenozoic lithospheric extension. The dikes in peridotite are parts of a complex system of conduits that fed magma to lower crustal intrusions represented by abundant xenoliths of the two youngest lithologic groups. Underplated igneous rocks of these two groups could comprise a section of 10–13 km thickness in the lower crust, as identified by seismic models, and be intercalated with peridotite through a maximum thickness of ~15 km below the Moho. All of the rocks comprising the green-pyroxene and Al-augite groups are considered to be new crustal additions, whether they come from above or below the Moho. The Moho is therefore not necessarily the crust–mantle boundary (Griffin & O'Reilly, 1987; Wilshire, 1990). Extensive remelting of both the dike rocks in peridotite and lower crustal components may indicate continuing decompression resulting from extensional deformation.

## REFERENCES

Albee, A. L., & Ray, A. L., 1970. Correction factors for electron probe microanalysis of silicates, oxides, carbonates, phosphates, and sulfates. *Anal. Chem.* **42,** 1408–14.

Beckerman, G. M., Robinson, J. P., & Anderson, J. L., 1982. The Teutonia batholith: a large intrusive complex of Jurassic and Cretaceous age in the eastern Mojave Desert. In: Frost, E. G., & Martin, D. L. (eds.) *Mesozoic–Cenozoic Tectonic Evolution of the Colorado River Region, California, Arizona, and Nevada.* National City, CA: Crest Offset Printing Co., 205–21.

Bence, A. E., & Albee, A. L., 1968. Empirical correction factors for the electron microanalysis of silicates and oxides. *J. Geol.* **76,** 382–403.

Best, M. G., & Brimhall, W. H., 1974. Late Cenozoic alkalic basaltic magmas in the western Colorado plateaus and the Basin and Range Transition Zone, U.S.A., and their bearing on mantle dynamics. *Geol. Soc. Am. Bull.* **85,** 1677–90.

Bodinier, J. L., Guiraud, M., Dupuy, C., & Dostal, J., 1986. Geochemistry of basic dikes in the Lanzo Massif (Western Alps): petrogenetic and geodynamic implications. *Tectonophysics* **128,** 77–95.

Boettcher, A., 1986. The relationship between alkali basalts (basanites) and gabbroic xenoliths in the Cima volcanic field, eastern Mojave Desert. *Geol. Soc. Am. Abstr. Prog.* **18,** 87.

Bohrson, W. A., & Clague, D. A., 1988. Origin of exsolved ultramafic xenoliths from Hualalai Volcano, Hawaii. *Contr. Miner. Petrol.* **100,** 139–55.

Boudier, F., & Nicolas, A., 1977. Structural controls on partial melting in the Lanzo peridotite. In, Dick, H. J. B. (ed.) *Magma Genesis. Bull. Oregon Dept. Geol. Miner. Indust.* **96,** 63–79.

Carswell, D. A., & Gibb, F. G. F., 1987. Evaluation of mineral thermometers and barometers applicable to garnet lherzolite assemblages. *Contr. Miner. Petrol.* **95,** 499–511.

Chatterjee, N. D., & Terhart, L., 1985. Thermodynamic calculation of peridotite phase relations in the system $MgO–Al_2O_3–SiO_2–Cr_2O_3$, with some geological applications. *Ibid.* **89,** 273–84.

Clague, D. A., & Dalrymple, G. B., 1987. The Hawaiian–Emperor volcanic chain. Part I. Geologic evolution. *U.S. Geol. Surv. Prof. Paper* **1350,** 5–54.

Coleman, R. G., 1984. The Red Sea: a small ocean basin formed by continental extension and sea floor spreading. *Proc. 27th Int. Geol. Cong., Moscow,* **23,** 93–121.

—— Gregory, R. T., & Brown, G. F., 1983. Cenozoic volcanic rocks of Saudi Arabia. *Saudi Arabian Deputy Ministry Miner. Res., Open File Rep.,* **USGS–OF–03–93,** 82 pp.

Colville, A. A., & Novak, G. A., in press. Kaersutite megacrysts and associated crystal inclusions from the Cima volcanic field, San Bernardino County, California. *Am. Miner.*

Downes, H., 1987. Relationship between geochemistry and textural type in spinel lherzolites, Massif Central and Languedoc. In: Nixon, P. H., (ed.) *Mantle Xenoliths.* New York: John Wiley, 563–74.

—— Dupuy, C., 1987. Textural, isotopic and REE variations in spinel peridotite xenoliths, Massif Central, France. *Earth Planet. Sci. Lett.* **82,** 121–35.

Finnerty, A. A., & Boyd, F. R., 1987. Thermobarometry for garnet peridotites: basis for the determination of thermal and compositional structure of the upper mantle. In: Nixon, P. H. (ed.) *Mantle Xenoliths.* New York: John Wiley, 381–402.

Gasparik, T., 1984. Two-pyroxene thermobarometry with new experimental data in the system $CaO–MgO–Al_2O_3–SiO_2$. *Contr. Miner. Petrol.* **87,** 87–97.

Gibbs, J. F., & Roller, J. C., 1966. Crustal structure determined by seismic-refraction measurements between the Nevada Test Site and Ludlow, California. *U.S. Geol. Surv. Prof. Paper* **550-D,** 125–31.

Green, D. H., & Ringwood, A. E., 1967a. The stability fields of aluminous pyroxene peridotite and garnet peridotite and their relevance in upper mantle structure. *Earth Planet. Sci. Lett.* **3,** 151–60.

———— 1967b. The genesis of basaltic magmas. *Contr. Miner. Petrol.* **15,** 103–90.

Griffin, W. L., & O'Reilly, S. Y., 1987. Is the continental Moho the crust–mantle boundary? *Geology* **15,** 241–44.

Gutmann, J. T., 1986. Origin of four- and five-phase ultramafic xenoliths from Sonora, Mexico. *Am. Miner.* **71,** 1076–84.

Harte, B., 1977. Rock nomenclature with particular relation to deformation and recrystallization textures in olivine-bearing xenoliths. *J. Geol.* **85,** 279–88.

Hauser, E. C., Gephart, J., Latham, T., Oliver, J., Kaufman, S., Brown, L., & Lucchitta, I., 1987. COCORP Arizona transect: strong crustal reflections and offset Moho beneath the transition zone. *Geology* **15,** 1103–6.

Hewett, D. F., 1956. Geology and mineral resources of the Ivanpah Quadrangle, California and Nevada. *U.S. Geol. Surv. Prof. Paper* **275,** 172 pp.

Himmelberg, G. R., & Ford, A. B., 1983. Composite inclusion of olivine gabbro and calc-silicate rock in the Dufek intrusion, a possible fragment of a concealed contact zone. *Antarctic J.U.S.* **18,** 1–4.

Hyndman, R. D., & Shearer, P. M., 1989. Water in the lower continental crust: modelling magnetotelluric and seismic reflection results. *Geophys. J. Int.* **98,** 343–65.

—— Klemperer, S. L., 1989. Lower-crustal porosity from electrical measurements and inferences about composition from seismic velocities. *Geophys. Res. Lett.* **16,** 255–8.

Irving, A. J., 1974. Geochemical and high pressure experimental studies of garnet pyroxenite and pyroxene granulite xenoliths from the Delegate basaltic pipes, Australia. *J. Petrology* **15,** 1–40.

—— Price, R. C., 1981. Geochemistry and evolution of lherzolite-bearing phonolitic lavas from Nigeria, Australia, East Germany and New Zealand. *Geochim. Cosmochim. Acta* **45**, 1309–20.

Jackson, M. D., & Ohnenstetter, M., 1981. Peridotite and gabbroic structures in the Monte Maggiore massif, alpine Corsica. *J. Geol.* **89**, 703–20.

Jaques, A. L., & Green, D. H., 1980. Anhydrous melting of peridotite at 0–15 kb pressure and the genesis of tholeiitic basalts. *Contr. Miner. Petrol.* **73**, 287–310.

Katz, M., & Boettcher, A., 1980. The Cima volcanic field. In: Fife, D. L., & Brown, A. R. (eds.) *Geology and Mineral Wealth of the California Desert.* Santa Ana: South Coast Geol. Soc., 236–41.

Klemperer, S. L., Hauge, T. A., Hauser, E. C., Oliver, J. E., & Potter, C. J., 1986. The Moho in the northern Basin and Range province, Nevada, along the COCORP 40 °N seismic-reflection transect. *Geol. Soc. Am. Bull.* **97**, 603–18.

McGuire, A. V., 1988. Petrology of mantle xenoliths from Harrat al Kishb: the mantle beneath western Saudi Arabia. *J. Petrology* **29**, 73–92.

Mysen, B. O., & Boettcher, A. L., 1975. Melting of a hydrous mantle: II. Geochemistry of crystals and liquids formed by anatexis of mantle peridotite at high pressures and high temperatures as a function of controlled activities of water, hydrogen, and carbon dioxide. *Ibid.* **16**, 549–93.

Nicolas, A., Lucazeau, F., & Bayer, R., 1987. Peridotite xenoliths in Massif Central basalts, France: textural and geophysical evidence for asthenospheric diapirism. In: Nixon, P. H. (ed.) *Mantle Xenoliths.* New York: John Wiley, 563–74.

O'Neill, H. S-C., 1981. The transition between spinel lherzolite and garnet lherzolite, and its use as a geobarometer. *Contr. Miner. Petrol.* **77**, 185–94.

O'Reilly, S. Y., & Griffin, W. L., 1985. A xenolith-derived geotherm for southeastern Australia and its geophysical implications. *Tectonophysics* **111**, 41–63.

Padovani, E. R., & Carter, J. L., 1977. Non-equilibrium partial fusion due to decompression and thermal effects in crustal xenoliths. In: Dick, H. J. B. (ed.) *Magma Genesis. Bull. Oregon Dept. Geol. Miner. Indust.* **96**, 43–57.

Pedersen, R. B., 1986. The nature and significance of magma chamber margins in ophiolites: examples from the Norwegian Caledonides. *Earth Planet. Sci. Lett.* **77**, 100–12.

Pike, J. E., & Schwarzman, E. C., 1977. Classification of textures in ultramafic xenoliths. *J. Geol.* **85**, 49–61.

Presnall, D. C., Dixon, S. A., Dixon, J. R., O'Donnell, T. H., Brenner, N. L., Schrock, R. L., & Dycus, D. W., 1978. Liquidus phase relations on the join diopside–forsterite–anorthite from 1 atm to 20 kbar: their bearing on the generation and crystallization of basaltic magma. *Contr. Miner. Petrol.* **66**, 203–20.

—— Hoover, J. D., 1987. High pressure phase equilibrium constraints on the origin of mid-ocean ridge basalts. *Geochem. Soc. Spec. Publ.* **1**, 75–89.

Reynolds, R. E., & Nance, M. A., 1988. Shadow Valley Basin: Late Tertiary deposition and gravity slides from the Mescal Range. In: Weide, D. L., & Faber, M. L. (eds.) *This Extended Land. Field Trip Guidebook.* Las Vegas, NV: Geol. Soc. Am., 207–9.

Turrin, B. D., Dohrenwend, J. C., Wells, S. G., & McFadden, L. D., 1984. Geochronology and eruptive history of the Cima volcanic field, eastern Mojave Desert, California. In: Dohrenwend, J. C. (ed.) *Surficial Geology of the Eastern Mojave Desert, California. Guidebook Geol. Soc. Am., 1984 Ann. Meeting, Field trip* **14**, 88–100.

Vaniman, D. T., Crowe, B. M., & Gladney, E. S., 1982. Petrology and geochemistry of hawaiite lavas from Crater Flat, Nevada. *Contr. Miner. Petrol.* **80**, 341–57.

Wells, P. R. A., 1977. Pyroxene thermometry in simple and complex systems. *Ibid.* **62**, 129–39.

Wilshire, H. G., 1987. Multistage generation of alkalic basalt in the mantle. *Geol. Soc. Am. Abstr. Prog.* **19**, 892.

—— 1988. Remelting of igneous and metaigneous rocks in the upper mantle. *EOS, Trans. Am. Geophys. Union* **69**, 1049.

—— 1990. Lithology and evolution of the crust–mantle boundary region in the southwestern Basin and Range province. *J. Geophys. Res.* **95**, 649–65.

—— Frisken, J. G., Jachens, R. C., Prose, D. V., Rumsey, C. M., & McMahan, A., 1987. Mineral resources of the Cinder Cones Wilderness Study Area, San Bernardino County, California. *U.S. Geol. Surv. Bull.* **1712-B**, 1–13.

—— Kirby, S. E., 1989. Dikes, joints, and faults in the upper mantle. *Tectonophysics* **161**, 23–31.

—— Meyer, C. E., Nakata, J. K., Calk, L. C., Shervais, J. W., Nielson, J. E., & Schwarzman, E. C., 1988. Mafic and ultramafic xenoliths from volcanic rocks of the western United States. *U.S. Geol. Surv. Prof. Paper* **1443**, 179 pp.

Windom, K. E., & Boettcher, A. L., 1981. Phase relations for the joins jadeite–enstatite and jadeite–forsterite at 28 kb and their bearing on basalt genesis. *Am. J. Sci.* **281**, 335–51.